

Università degli studi di Padova
centro interdipartimentale Centro Ricerche Fusione
Universidade de Lisboa
ISTITUTO SUPERIOR TECNICO

JOINT EUROPEAN RESEARCH DOCTORATE IN FUSION SCIENCE AND ENGINEERING
Cycle XXXI

Development of a fiber-optics polarization resolving THz spectrometer for harsh environment diagnostics application

Coordinator:
Prof. Paolo Bettini

Supervisors:
Dr. Marco Zerbini
Dr. Flavio Crisanti

Ph.D. Student: Giuseppe Galatola Teka

ABSTRACT

The measurement of the physical parameters required to define the dynamic of a thermonuclear plasma is of fundamental importance to the advancement of new generation experimental Fusion reactors.

In the last twenty years, the development in sources and detection systems filled the so called "THz Gap", making available the electromagnetic bandwidth between 0.1 and 20 THz for a wide range of experimental applications.

The applications of THz radiation to Fusion Plasma Diagnostic, by using the TeraHertz Time Domain Spectroscopy (THz-TDS) has been pursued since 2011.

This technique bears some similarity with Radar applications and utilises picosecond pulse with wide spectral bandwidth to analyze spectral characteristics of a variety of samples. This Ph. D. thesis was devoted to the application of this technique to a set of well established plasma diagnostics: interferometry, reflectometry and polarimetry, to be replaced by a single multifunctional THz-TDS instrument.

A THz-TDS spectrometer is based on a femtosecond (fs) laser in the near infrared (800 nm) which by illuminating a specific kind of semiconductor (like GaAs) generates a THz pulse. The detection of the pulse is achieved with the inverse process.

The appeal of the diagnostic is also given by the possibility to transport the infrared laser pulse with fibre optics a long way, to the emission and detection heads, overcoming the notorious access problems in Tokamaks.

During the three years work, the activity was divided into two branches: construction and optimization of a THz-TDS set

up in Frascati to determine the final characteristic of a plasma diagnostic test facility, and the completion of a number of plasma-diagnostics relevant laboratory tests.

The thesis is organised as follows:

In the first chapter, the work domain of the thesis is presented within the fields of Nuclear Fusion experiments and the state of the art THz technology is briefly introduced: sources, detectors and applications.

In the second chapter, the main diagnostic techniques in the FIR and submillimeter range are discussed by using the classical electromagnetic propagation theory in plasma. The possible applications of THz-TDS to achieve the same kind of measurement for plasma density and poloidal magnetic field are developed.

In the third chapter, the THz-TDS technique is described in detail with specific reference to the experimental devices developed and utilized in the Frascati laboratory.

In the fourth chapter, the experimental tests relevant for the construction of the diagnostic are shown and discussed . Two types of detector are used in the tests (Electro Optical and Photoconductive). The application of optical fibers to the IR laser propagation is then discussed and experimentally studied. Finally the basic algorithms and models for spectroscopic data analysis have been developed and tested with the relevant experimental data.

The fifth chapter summarizes conclusions and future work.

SOMMARIO

Individuare i parametri fisici adatti a determinare lo stato della dinamica di una plasma termonucleare e' d'importanza fon-

damentale nello sviluppo dei reattori sperimentali di nuova generazione.

Negli ultimi venti anni lo sviluppo di sorgenti e di sistemi di rivelazioni ha permesso di colmare quello che veniva prima definito Gap THz, permettendo di utilizzare la porzione dello spettro elettromagnetico dai 0.1 ai 20 THz.

Nel centro ricerce di ENEA Frascati si e' deciso di studiare l'applicabilita' della radiazione THz al campo delle diagnostiche per lo studio delle proprieta' del plasma termonucleare, nello specifico attraverso la tecnica della Time Domain Spectroscopy (THz-TDS).

Questa tecnica di principio simile alla tecnica radar, utilizza impulsi al picosecondo con un ampia larghezza spettrale per poter analizzare materiali. Questo progetto di dottorato si e concentrato nello sviluppo della strumentazione adatta allo studio di una possibile diagnostica di questo tipo per poter affiancare e si progetta, successivamente, sostituire una serie di diagnostiche come l'interferometria, la riflettometria e la polarimetria con un singolo strumento.

Un sistema THz-TDS e' costituito da un laser che produce impulsi dell'ordine del femtosecondo nella regione del vicino infrarosso (800 nm) che investendo un opportuno semiconduttore (per esempio GaAs) genera per fotoconduzione impulsi THz. La rivelazione avviene in maniera simile, tramite il processo inverso.

La diagnostica ha la sua attrattiva anche nella possibilita' di poter trasportare l'impulso infrarosso alle teste di emissione e ricezione THz a molti metri di distanza utilizzando fibre ottiche.

Durante i tre anni di lavoro l'attivita' si e' concentrata su due filoni principali: la costruzione e ottimizzazione di un sistema THz-TDs nei laboratori di Frascati al fine di determinare le ca-

ratteristiche ottimali di un sistema da utilizzare per diagnostiche del plasma e l'effettuazione di prove di laboratorio rilevanti per le misure di plasma.

La tesi si articola come segue.

Nel primo capitolo vengono specificati il dominio del lavoro nell'ambito degli esperimenti di fusione nucleare e lo stato dell'arte della tecnologia THz: sorgenti, rivelatori e applicazioni.

Nel secondo capitolo si utilizza la trattazione classica della propagazione di onde elettromagnetiche nel plasma per descrivere le principali diagnostiche in ambito FIR e submillimetrico, e la possibilita di applicazione della spettroscopia THZ-TDS per ottenere lo stesso tipo di misure di densita e campo magnetico poloidale del plasma. A titolo applicativo le applicazioni diagnostiche vengono discusse in relazione al Tokamak FTU di Frascati.

Nel terzo capitolo si descrive la tecnica THz-TDS e si illustrano le componenti dell'apparato sperimentale utilizzato nel laboratorio di Frascati.

Nel quarto capitolo si mostrano i test sperimentali effettuati durante il lavoro di dottorato, dalla costruzione della diagnostica, con lo studio di due tipologie di detector e le basi per l'applicazione in fibra della tecnica fino agli studi degli algoritmi e dei modelli adatti a validare la diagnostica per lo studio di plasmi. Il quinto capitolo e' costituito dalle conclusioni ed i progetti futuri.

Resumo

Individuar os parâmetros físicos adequados para determinar o estado da dinâmica de um plasma termonuclear é de fundamental importância para o desenvolvimento dos reatores experimentais de nova geração.
Nos últimos vinte anos o desenvolvimento de fontes e de sistemas de revelação permitiu de preencher o que era antes definido Gap THz, permitindo de usar a porção do espectro eletromagnético dos 0.1 aos 20 THz.
No centro de pesquisas do ENEA em Frascati se decidiu estudar a aplicabilidade da radiação THz ao campo das diagnósticas para o estudo das propriedades do plasma termonuclear, específicamente através da técnica da Time Domain Spectroscopy (THz-TDS).

Essa técnica de princípio semelhante à técnica radar, utiliza impulsos ao picossegundo com uma ampla largura espectral para poder analizar materiais. Este projeto de Doutorado se concentrou no desenvolvimento de instrumentação adequada ao estudo de uma possível diagnóstica deste tipo para poder ajudar, e se projeta sucessivamente substituir, uma série de diagnósticas como a interferometria, a reflectometria e a polarimetria com um único instrumento.

Um sistema THz-TDS é composto de um laser que produz impulsos da ordem do femtosegundo na região do vizinho infravermelho (800 nn) que investindo um adequado semicondutor (por exemplo GaAs) gera através da fotocondução impulsos THz com banda espectral larguissima (100 GHz - 10 THz). A revelação ocorre de modo semelhante através do processo inverso.
A diagnóstica é também interessante pela possibilidade de poder transportar o impulso infravermelho às testas de emissão e recepção THz a muitos metros de distância utilizando fibras óticas.
Durante os três anos de trabalho a atividade se concentrou sobre dois filões principais: a construção e otimização de um sistema THz-TDs, nos laboratórios de Frascati, com o objetivo de determinar as melhores caracteristicas de um sistema a ser utilizado para a diagnóstica do plasma e a realização de provas de laboratório para as medidas de plasma.

A tese se desenvolve como segue:

No primeiro capítulo veem especificados o domínio do trabalho no âmbito dos experimentos de fusão nuclear e o estado da arte da tecnologia THz: fontes, reveladores e aplicações.
No segundo capítulo se utiliza o tratamento clássico da propagação de ondas eletromagnéticas no plasma para descrever as principais diagnósticas em âmbito FIR e submilimetrico e a possibilidade de aplicação da espectroscopia THZ-TDS para obter o mesmo tipo de medidas de densidade e campo magnético poloidal do plasma. A título aplicativo as aplicações diagnósticas veem discutidas em relação ao Tokamak FTU de Frascati.

No terceiro capítulo se descreve a técnica THz-TDS e se ilustram as componentes do aparelho experimental utilizado no laboratório de Frascati.
No quarto capítulo se mostram os testes experimentais efetuados durante o trabalho de Doutorado, da construção da diagnóstica com o estudo de duas tipologias de detector e as bases para a aplicação em fibra da técnica até os estudos dos algoritmos e dos modelos adequados à validação da diagnóstica para o estudo dos plasmas.

O quinto capítulo é constituído das conclusões e dos projetos futuros.

No apêndice se descreve a instalação da diagnóstica interferométrica laser a segunda armonica na máquina Proto Sphera e as primeiras medidas de plasma efetuadas sobre a mesma que, como parte integrante do projeto de realização diagnóstica deste Doutorado, permitiu uma familiarização e uma compreensão das problemáticas experimentais relacionadas com este tipo de aplicações.

CONTENTS

LIST OF FIGURES

LIST OF TABLES

1

NUCLEAR FUSION AND THE ROLE OF THZ-SPECTROSCOPY IN PLASMA DIAGNOSTICS

1.1 NUCLEAR FUSION

One of the challenges of the last century was, and still is, the research for systems that can deal with the increasing demand of energy of the Industrial and post Industrial society. In recent years, the concern about the environmental issues raised by the energy production through coal, oil and nuclear fission led to research into alternative means of energy production. One of the strategies to overcome the energy demand is to utilise nuclear fusion, as it is an attractive source of energy in terms of safety, fuel reserves and minimal damage to environment [1]. The nuclear fusion principle consists in combining two particles into a heavier one. As a result of the overall reaction, part of the total mass of the colliding particles is converted in kinetic energy . The most common fusion reaction in nature is the proton-neutron fusion in the stars. The high pressure, generated by the extreme gravitational forces exerted by the mass of the stars, makes this reaction thermodynamically favourable. On Earth, since it is not possible to achieve a similar activation energy, deuterium, which occurs plentiful in nature, is a possible candidate to be used as fuel in a fusion energy production facility. In these conditions, the lowest activation energy is achieved when the fusion reaction is between deuterium and

tritium, a rare radioactive material.These two particles can react according the two reactions shown below:

$$^{2}_{1}H + ^{3}_{1}H \rightarrow ^{4}_{2}He + n^{0} + 17.6MeV \quad (1)$$

$$^{2}_{1}H + ^{2}_{1}H \rightarrow ^{3}_{2}He + n^{0} + 3.27MeV \quad (2)$$

In controlled nuclear fusion the Coulomb energy repulsion barrier between two nuclei must be overcome to have the short-range nuclear attraction dominant. To achieve this fusion, the particles n_e must retain their energy (expressed in function of the temperature T_e) for a sufficient period of time τ_e to obtain a positive balance. This principle can be summarized by the Lawson Criterion [2]:

$$n_e \tau_e T_e \geqslant 1.2 \times 10^{21} m^{-3} \cdot keV \cdot s \quad (3)$$

The process utilized in the research to supply the particles of this energy is to heat them with various process (Ohmic, NBI, ECRH) [3] . The operational temperature is about 10 KeV, which is less than the maximum cross-section temperature, because the reactions occur in the tails of the Maxwellian distribution of heated particles. At this temperature the energy is enough to fully ionize the matter and to let it remain in the state of plasma. Since no material can resist to the direct contact with the high temperature plasma, the principle of magnetic confinement is exploited to oblige charged particles to follow the magnetic force lines oriented in order to not collide with the walls of the machine. The most used configuration of magnetic field is the Tokamak (Fig 1). Invented in the 1950 in Russia, The Tokamak utilises two magnetic fields: an external toroidal field generated by the winding of a transformer, and an inter-

nal poloidal field generated by the plasma current (induced by the transformer) to overcome the plasma pressure. The resulting combined magnetic field gives rise to helicoidal magnetic lines.

Current Tokamaks work with particle densities of $10^{19} - 10^{20}$, with operational Ohmic temperatures of a few KeV and fusion temperatures achieved with additional heating [3].

The Tokamak's plasma exhibits relevant optical properties in the region of the millimetre and sub millimetre [5] electromagnetic waves, leading to the development of various diagnostics tools capable to extract physical parameters of the dynamics of operation of the Tokamak, like density profiles and magnetic field profiles providing information on the magnetic equilibrium of the machine [6].

The objective of this doctoral thesis is to lay the first experimental basis for developing a diagnostic instrument which utilises novel THz technologies, to study optical plasma properties and so develop a new Plasma diagnostic tool.

1.2 THZ TECHNOLOGY

In the last few decades the spectral region ranging from 0.1 to 60 THz (3 mm - 0.03 mm), usually called "THz gap" shown in Fig. 2, has been extensively studied, with a major development in the sources and detectors [7].

One of the main experimental setups and measurement techniques is THz time-domain spectroscopy (TDS) can investigates the spectral propriety of a media in transmission and reflection with a simple procedure both in the theoretical and experimental applications. The advancement in femto-seconds IR Laser technology has provided the possibility to utilise frequencies conversion media like semiconductor and electroptic crystal, to

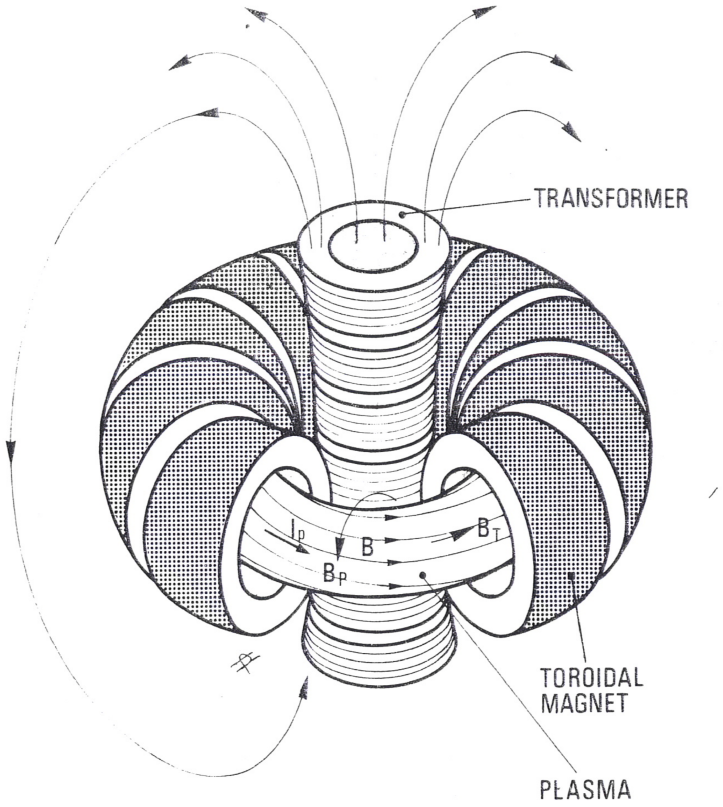

FIG. 1 TOKAMAK CONFIGURATION

Figure 1: Tokamak layout, from original historical reference [4] by L.Pieroni.

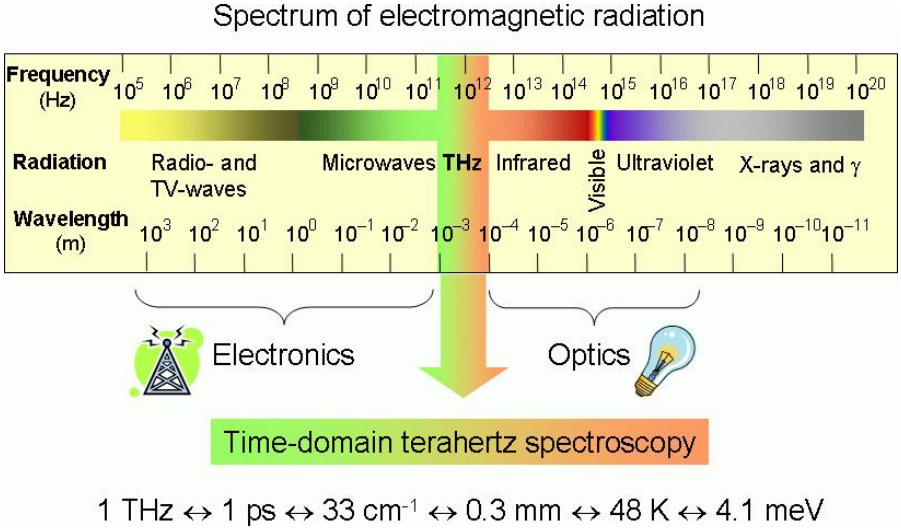

Figure 2: Position of the THz gap in the electromagnetic spectrum. Taken from http://lts.fzu.cz/en/intro.htm

produce picosecond pulses, that have a THz frequency bandwith [8]

With THz-TDS spectroscopy it is possible to study the scattered, reflected and absorbed frequency of an element. The THz radiation with its millimetre wavelength, low energy non-ionizing photons ($k_B T$=75 meV) is a useful spectral range that lies between the electronic and the optical ranges. In the last sixty years the leading spectroscopic system in various fields was the interferometer. The interferometer gives a signal called an interferogram [9] that can be converted in a frequency spectrum by Fourier analysis in which the main advantage is the high throughput and spectral sensitivity within a narrow bandwith. In the last decades, THz Time Domain Spectroscopy (THz-TDS) has emerged as an alternative to the interferometer for spectrocopic study. With this technique narrow bandwidth spectroscopy measurement are possible with only one measurement and instrument.

The THz spectral region has been investigated utilising several approaches and physical phenomena , all with merits and

drawbacks. To the best of the authors knowledge, a full THz bandwidth (0.1 to 200 THz) is not possible with a single instrument as continuos emission and detection throughout the whole THz range, can only be achieved using different kind of source and detectors each with different (and smaller) bandwidth. The main sources of THz radiation (or T beams) investigated in the recent years will be discussed in the following sections.

1.2.1 *The generation of THz radiation*

THERMAL EMISSION The ideal emitter is the blackbody radiator (eq. 4) [10] . In laboratory spectroscopy, it is possible to have sources that typically vary between 1000 and 5000 k which emit radiation in the THz range. The spectral emission density of a Black Body is expressed by:

$$B_\nu^{RJ} d\nu = \frac{2k_B T \nu^2}{c^2} d\nu\nu \tag{4}$$

with k_b the Boltzman costant, T the temperature ν the frequency and c the light velocity.

Globar [11] have sufficient emissivity at THz frequencies, although only above 3 THz. They consist of cylindrical rods of silicon carbide caped with metallic electrodes, and a water-cooled housing with a slit allowing light emission; with operating temperature of 1360-1500 K and emissivity 0.85 in the visible and near IR. Another practical approach is to utilise arc lamps and the radiation emission of plasma (hot gas) or plasma lamps. One of the most used is the mercury arc lamp [11], composed by a quartz bulb that contain the electrodes which produces the plasma. If the temperature of the plasma is 5000 K and the the quartz bulb temperature is 1000 K the arc lamp produces

stable and homogeneus radiation below 3 THz with increasing radiation absorption above 1 THz till complete absorption at 3 THz due to quartz envelope leading to emissivity 0.88 in the THz range.

GAS LASER According to the laser theory, it is possible to find a Gas with the right quantum energy level for emission in the THz regime and good quantum energy inversion properties. To excite the molecules of the gas, it is possible to use two different mechanisms: (1) Electrically excited Gas lasers, which utilise the glow discharge in pure gases, usually H_2O, D_2O or H_2S, enclosed in a Fabry-Perot cavity, that are simple in construction, to produce a variety of CW and pulsed laser with frequencies in 1-1.5 THz range with power up to 600 mW [12]. (2) Optically excited Gas lasers, usually CO2, which have radiation emission from 0.15 THz to 8 THz with output power raging from several μW to several hundreds of mW. The lack of significant frequency tunability, which is due to the nature of the active medium that ultimately limits its use.

PHOTOMIXING FOR THE GENERATION OF TERAHERTZ RADIATION Electromagnetic waves with different frequencies generate sum and difference of frequencies in an element with a non linear I-V curve or any other nonlinear element as ZnTe crystal, GaAs semiconductors or QLC cavities. . For a fast response of the emitter material in the THz regime, a relaxation time of the photo carriers of less than 1 ps is required [8].

SEMICONDUCTOR LASER The photon emission is due to electron hole recombination in semiconductor such as (GaAs, InAs). These are usually inefficient in the THz range because the band exceeds 18 THz and the inversion of population is

difficult to achieve because the equivalent temperature of the energy gap is comparable to room temperature (300 K) .

Nevertheless utilising a special mechanism that support laser action in the between of the Landau Levels due to magnetic interaction a new type of semiconductor laser, and so there is an emission from similar narrow bandwidth quantum level, with one photon for quantum well, called Quantum Cascade Lasers (QCL) was developed [13]. QCL are semiconductor laser that can emit high amplitude laser beam at fixed frequency in the order of the THz. Particular is the capacity of be a tunable laser with narrow bandwidth emission between 1.2 to 4.9 THz with lower bandwidth of 10 GHz and output of 140 mW.

PHOTOCONDUCTIVE ANTENNAS First applied in the 80's in the work of Auston [14], it utilizes a semiconductor (usually GaAs or InAs) photo-excited by a fs laser pulse, biased by an Electric Field to produce electromagnetic pulses, in a way similar to the dipole effect. A generic setup is one were two stripes or a bowtie antenna (usually gold) are positioned by lithography over the semiconductor slab, with separation from tens to hundreds of micron and biased with voltage of about 10 V. The typical bandwidth produced is 5 THz, the power is on the order of tens mW and DR is about 60 dB [15].

MAGNETIC FIELD ENHANCEMENT A way to increment the output of a semiconductor emitter is to apply a magnetic field in the range of 1 to 7 T at a perpendicular angle to the surface of the semiconductor. The magnetic field accelerates the carriers by Lorentz force perpendicular the surface plane, leading to a component of acceleration, and consequently a current in the transverse direction increasing the compatibility for the THz propagation at the dielectric/air interface [16]. This effect rein-

force the THz pulse generation power, to a maximum 450 μW, but with a similar SNR to the photoconductive Antennas.

LARGE-APERTURE ANTENNAS One use of amplified lasers is to photo excite antennas that have a wider separation between the electrodes [17]. These have a transverse dimension that is large relative to the spatial duration of the fs pulse, allowing a non-focused operation of the laser that otherwise would lead to the destruction of the standard small gap antennas. The drawback is that a bias tension ten times greater than used in small gap emitters has to be applied. Characteristic pulse energy are 0.8 μJ/pulse with amplitudes that scale linearly with bias voltage and increase until saturation of disponibile charges.

OPTICAL RECTIFICATION Another way to use amplified laser is to use optical rectification of nonlinear medium [18] , [19] like ZnTe or GaP crystals. When the light of the laser interacts with the non-linear medium, the optical rectification is the difference frequency, a non-resonant method, based on the study of the polarization of a dieletric media as shown in (equation 5), limited by the power injected and by the energy absorption breakdown limits of the material. This can be represented by a mix of the high frequency component with the low frequency one to produce a pulse in which the frequencies difference is on the order of the THz. One area of interest is the generation of high bandwidth radiation, with notable example in [18] , [19] where full spectral coverage until 60 THz was obtained with a partial spectral coverage due to phonon modes of the electro optical components that produce some frequencies gap in the emission spectra.

$$P(E) = \epsilon_0 \chi^{(1)} E + P^{NL} \tag{5}$$

$$P(E) = \epsilon_0 (\chi^{(1)} E + \chi^{(2)} E + ...) \tag{6}$$

with P(E) the polarization of the dielectric and $\chi^{(n)}$ the Taylor expansion of the susceptibility coefficents that permits to explain the linear and non linear effects of the media (as photomixing).

SYNCHROTRONS AND FREE ELECTRON LASERS Synchrotrons and free electron lasers can generate short pulses of far infrared radiation on the order of 5-10 ps with sub picosecond pulses in the latest generation FEL [15]. They use an electron beam accelerated at relativistic energy interacting with a magnetic field. They have a broad tunability and high power levels with low temporal resolution and high cost.

LASER GENERATED PLASMAS When an intense laser pulse is focused in air (or other gases) Radiation up to 4 THz is generated by the ponder-motive force, applied bias voltage across the air gap or non-linear four wave mixing. The main advantage is the absence of phonon absorption [20].

1.2.2 *The detection of THz radiation*

There is a wide range of physical effects, which can be used in detection systems [21]. The majority of these can be conveniently categorized into four main groups [8]:

THERMAL DETECTORS These detectors convert the absorbed radiation in heat, that can be easily measured as a

temperature increase ΔT. The most used kind of detectors are Bolometer, which convert the heat directly into a variation of electrical resistance, and Golay Cell detector where the heat is converted in gas expansion variation, that can be measured and converted into an electrical signal. They use a proved physical mechanism, easy to understand, but they have a little spectral resolution, absorbing a wide spectral range.

PHOTODIODES DETECTORS Photons at THz frequencies are absorbed and generate an electron current, that can be measured as a resistance variation. In this semiconductors based detectors is present gap between the valence and conducting band. When a photon with energy greater than the gap impriges the semiconductor, an electron become excited from the valence to the conduction band producing an extra electron (Intrinsic excitation). If the energy of the photon is not sufficent to excite the gap is possible to cause a photoconductive process by adding impurities to the semiconductor (Extrinsic excitation).

HETERODYNE DETECTION If currents of two different but closely spaced frequencies and in phase beat in the same electric circuit they will produce new frequencies, sum and difference frequencies, as well as harmonic; this process is called heterodyne. A heterodyne receiver is optimized for the detection of one of the two "beat" signal for example the difference frequency, typically a few GHz for a THz heterodyne receiver.

OTHERS The photoconductive antenna and the electro optic sampling (E.O. or EO), are the source and detection elements used during the Ph. D. work and follow a physical process similar to the one explained in section 1.2.1 which will be further explained the paragraph (3.3.2) of this thesis.

1.2.3 *Applications of THz radiation*

In the past few years THz-TDS, has shown capability as useful material spectrometers that could compete with the use of the IR interferometer spectrometer. They were used to inspect a variety of elements that will be summarized briefly below and are presented in detail in the THz 2017 road map [22]

SEMICONDUCTORS THz-TDS optical-pump terahertz-probe (OPTP) spectroscopy is used to investigate ultrafast carrier photoconductivity. The main advantage is it the non-contact probe of electrical conductivity with sub-picosecond temporal resolution, for example the study of GaAs electron-hole dynamic which are particularly successful [22].

BIOLOGICAL APPLICATIONS THz radiation is a useful technique due to strong absorption of the water molecules and resonance of biomolecules in THz range, as well as low energy of THz photons wich reduce the tissue damage. THz can therefore distinguish between healthy and unhealthy or damaged tissues. On the other end DNA molecules have the intramolecular vibrations in the THz range so that their collective motion and thus their function can be analyzed. Numerous groups have now demonstrated medical applications in breast, skin and colon cancer, and corneal hydration. Measurements similar to ultrasound imaging allow using the reflection to study the internal structure of semi-transparent media. They permit also to observe the hydrogen bonding in the molecules and allow to study new type of compounds.

TERAHERTZ COMPONENTS AND SYSTEMS FOR DEFENCE AND SECURITY IMAGING THz has now been used in dis-

tant security instrument that from meters away can screen crowd as standard airport security elements. The major benefits are: miniaturization of the hardware (components scale with wavelenghts) with wider deployment opportunities, high information content with the high bandwidth spectrum (especially for communication) and the vast selection of molecular vibrations and similar marker that can be used to identifies elements.

THZ COMMUNICATIONS It is expected that global wireless communication data will arrive to 24.3 Exabite in 2019 [22]. A new wireless communication technology is needed to support this quantity of data and to expedite transfer. THz range is investigated to support a much wider band of data transmission (0.1-10 THz) than the one used nowadays with the Wi-fi protocols, from 2 to 5 GHz, and is characterized by a more critical directional alignment.

METROLOGY FOR THZ TECHNOLOGIES THz technology has matured to a level that now is frequently used as for metrology and standardization. Free space Time domain spectrometry is used as characterisation of dielectric constant of material as well as free space Fourier transform spectrometer for ultra wide band measurement that overlaps the sub THz and the mid IR. Waveguide THz technology are predominantly made using heterodyne vector network analyzer (VNA) based systems, and enable coherent detection and standard calibration procedures.

THESIS APPLICATION The application of mature THz-TDS methods to the Plasma Diagnostics environment will allow us to realise a new concept instrument enabling multiple measure-

ments with one single diagnostic tool across a wide FIR spectral range (i.e. reflectometry, interferometry, polarimetry, ECE suprathermal emission). The TDS spectrometry instrumentation has a higher level of flexibility which can be exploited to adapt it to the mechanically and physically harsh and complex Tokamak environment, while the use of optical fibers will ease up physical access to the plasma. Most of the aforementioned THz sources presents only one frequency emitted, as the QCL and Gas Laser, while a wide spectrum was needed. The thermal sources produced a wider range of spectrum but the PCA pulse generation is fundamental for TDS application PCA where prefered to Plasma THz emition and Free Electron laser because them cannot be put easily near a tokamak facility and a simple and easy to use set up, with fiber optics and PCA emitter and detector was chosen. Similar reasoning can be applied to the detector choice.

2

PLASMA DIAGNOSTIC WITH ELECTROMAGNETIC WAVES

2.1 PLASMA DIAGNOSTIC POTENTIAL

The routine operation of a fusion test facility requires the knowledge of many specific physical parameters, such as the density of electron particles, their temperature and magnetic fields. The branch of physics that studies how to extract them is called "plasma diagnostics". The interior of the experimental machine is one of the harshest environments present on earth: temperatures on the order of thousands of eV, intense neutron flux and 1-10 T magnetic fields all prevent the use of *in-situ* physical probes, for an indirect way to measure the above mentioned physical parameters. Electro-magnetic waves (EMW) of sufficiently low energy which ensures that the proprieties of the plasma are not modified, are a feasible solution for an indirect probe: by studying how their amplitude and phase are affected by the plasma it is possible to deduce its physical parameters.

There are two major diagnostic techniques in which EMW are utilised: the active probe i.e. sending the EMW from an external antenna in vacuum to the plasma, and the passive probe i.e. observing the radiation emitted from the plasma itself. The propagation inside the plasma of EMW works in the same way for both approaches and the mathematical formulation of this propagation will be outlined in the next paragraph.

2.2 THE REFRACTION INDEX OF THE PLASMA

Using Fourier methods, a stationary EMW can be linearised into a sum of monochromatic waves in the form $Ae^{i(kr-\omega t)}$. Defining ω as the angular frequency and $\vec{k}$ as the wave vector, it is possible to define the relation between them as:

$$k = \frac{\omega}{c}\tilde{N} = \frac{\omega}{c}(n + iq) \tag{7}$$

Where $\tilde{N}$ is the complex index of refraction of the plasma and n and q are the real index of refraction and q the coefficient of extinction index (often denoted as the absorption index of k) and c the speed of light [6], [23].

The derivation of $\tilde{N}$ starts from the four Maxwell equations related to current flow in the plasma, modelled by a continuous medium.

$$\vec{\nabla} \cdot \vec{E} = \frac{\rho}{\epsilon_0} \tag{8}$$

$$\vec{\nabla} \cdot \vec{B} = 0 \tag{9}$$

$$\vec{\nabla} \wedge \vec{E} = -\frac{\delta \vec{B}}{\delta t} \tag{10}$$

$$\vec{\nabla} \wedge \vec{B} = \mu_0 \vec{J} + \mu_0 \epsilon_0 \frac{\delta \vec{E}}{\delta t} \tag{11}$$

By taking the curl of the equation (8) and the temporal derivative of the equation (9) it is possible to unify the two Maxwell equations in (12) [23]:

$$\vec{k}\vec{k}\vec{E} - k(k \cdot \vec{E}) + \frac{\omega^2}{c^2}\vec{\epsilon} \cdot \vec{E} = 0 \tag{12}$$

ϵ_0 and μ_0 are the permittivity and the permeability in vacuum and ϵ is the permettivity in the element. As above, Fourier

is applied to the tensor equation that describes the EMW propagation and this system is modelled with a 3X3 vector matrix. Nullifying its determinant it is possible to obtain the index of refraction, if the transverse wave dispersion relation is known [6].

$$\vec{k}\vec{k} - k^2\mathbf{I} + \frac{\omega^2}{c^2}\vec{\epsilon} = \begin{bmatrix} -k^2 + \frac{\omega^2}{c^2}\epsilon & 0 & 0 \\ 0 & -k^2 + \frac{\omega^2}{c^2}\epsilon & 0 \\ 0 & 0 & \frac{\omega^2}{c^2}\epsilon \end{bmatrix} \tag{13}$$

$$-k^2 + \frac{\omega^2}{c^2}\epsilon = 0 \tag{14}$$

$$\frac{\omega^2}{c^2} = 0 \tag{15}$$

As is shown in equation 14, the index of refraction is dependent directly on the dieletric tensor of the plasma. There are many methods of deriving plasma conductivity, from the simplest approaches to more sophisticated theories. The approach using kinetic theory is a simple yet adequate method in describing this phenomenon.

A customary starting ground in the description of wave propagation is an infinite, uniform Lorentz plasma, a simplified model which assumes that the electrons interact with each other through collective effects of continuous distribution of charges, known as space charge forces, and that the ions can be considered at rest. A further used hypothesis, called "cold" plasma approximation, is when we can neglect the effects which have an explicit dependency on electron temperature.Our model has to be named more appropriately "warm" since T_e is not assumed to be zero, but the required condition is

equivalent to the "cold" state when the velocity of the particle is orders of magnitude less than the speed of light in the plasma.

From first principles it is possible to obtain the dielectric tensor:

$$\vec{\epsilon} = \begin{bmatrix} 1 - \frac{\omega_p^2}{\omega^2 - \Omega^2} & \frac{i\omega_p^2 \Omega}{\omega(\omega^2 - \Omega^2)} & 0 \\ -\frac{i\omega_p^2 \Omega}{\omega(\omega^2 - \Omega^2)} & 1 - \frac{\omega_p^2}{\omega^2 - \Omega^2} & 0 \\ 0 & 0 & 1 - \frac{\omega_p^2}{\omega^2} \end{bmatrix} \tag{16}$$

substituting the above into equation (13) it is possible to obtain the reduced form of the determinant

$$\begin{bmatrix} -N^2 + 1 - \frac{X}{1-Y^2} & \frac{iXY}{1-Y^2} & 0 \\ -\frac{iXY}{1-Y^2} & -N^2 cos^2\theta + 1 - \frac{X}{1-Y^2} & N^2 sin\theta cos\theta \\ 0 & N^2 sin^2\theta cos\theta & -N^2 sin^2\theta + 1 - X \end{bmatrix} = 0 \tag{17}$$

Under these hypotheses, the refractive index of a cold plasma immersed in a uniform magnetic field B, for waves of radian-frequency ω propagating at an angle θ with respect to B, is given by the Appleton-Hartree formula [6]:

$$N^2 = 1 - \frac{X(1-X)}{1 - X - \frac{1}{2} \pm [(\frac{1}{2}Y^2 sin^2\theta)^2 + (1-X)^2 Y^2 cos^2\theta]^{\frac{1}{2}}} \tag{18}$$

where $X = \frac{\omega_p^2}{\omega^2}$ and $Y = \frac{\Omega}{\omega}$ and $\omega_p = \sqrt{\frac{n_e e^2}{\epsilon_0 m_e}}$ and $\Omega = \frac{eB}{m_e}$ are the plasma frequency and the cyclotron frequency respectively, expressed in terms of the elementary electrical charge e, the electron density n_e, the permittivity of free space ϵ_0 and the electron mass m_e. The $\pm$ sign accounts for the two polarisations of the wave, defined as:

- Ordinary mode E parallel to B

- Extraordinary mode E perpendicular to B

The above equation becomes suitably manageable when only the propagation components perpendicular to the magnetic field **B** are considered, hence $\theta = \frac{\pi}{2}$ with notable major cases:

$$N^2 = 1 - X \tag{19}$$

$$N^2 = 1 - \frac{(X(1-X))}{(1-X-Y^2)} \tag{20}$$

With equations (19 , 20) respectively defined as Ordinary or O-mode and Extraordinary or X-mode.

In order to apply the above derivations to our system, the requirement is that the plasma properties vary sufficiently slowly ($|\vec{\nabla}\vec{k}|/k^2 << 1$), allowing the EMW to be modelled locally as a wave propagating in an approximately uniform medium.

Thus, for any frequency and propagation direction, there exists locally a well defined k and refractive index N corresponding to the local values of the plasma parameters.

It is useful to define a specific frequency with a special property: the cut-off frequency, where in O mode the wave is perfectly reflected. This reflection takes place when the density of the plasma is such that the plasma frequency is equal to the incoming EMW frequency. In X mode the two definined frequency limiting values are the lower and upper hybrid frequency, where the EMW frequency is equal to the ciclotron frequency, upon which wave absorption occurs. There are two well known limit cases for refractive index N [24]:

- Cut-offs: $N \to 0$, $\lambda \to \infty$ wave reflected, transmission damped, $N^2 < 0$ after cut-off
- Resonance: $N \to \infty$, $\lambda \to 0$ wave absorbed

By setting N=0 in equation (20)

the following cut-off frequencies are obtained:

- $\omega = \omega_p$ Ordinary Mode cut-off
- $\omega_{(R,L)} = \sqrt{\frac{\omega_{ce}^2}{4} + \omega_{pe}^2 \pm \frac{\omega_{ce}}{2}}$ Extraordinary Mode cut-offs (+=R, -=L)

L, R are called Left and Right cut-offs. Note that if there is no magnetic field $\omega_{ce} = 0$ and all the cut-offs are reduced to the O-mode one.

The names of Wentzel, Kramers, and Brillouin (and sometimes Jeffreys, in what follows WKBJ [25]) have become associated with a widespread technique for solving such wave-type equations in slowly varying media; the scale of the uniformity of the plasma is larger than the effect (wavelenght and frequency) of EMW so that is possible to continue to use the homogeneous plasma formalism of equations resolution . The approach is also known as the Eikonal approximation, or more simply the geometric optics approximation.

In the core of active probing three are the most commonly used diagnostics: interferometry, polarimetry and refractometry. These are applied to the determination of average quantities on the line of sight of the diagnostic.

2.2.1 *Interferometry*

As seen in the equations 20 the plasma possesses a well defined index of refraction and an EMW propagating through the plasma will undergo a phase shift.

An interferometer uses two or more coherent waves, known as branches, and studies the variation of their interference. The two main used configurations are the Michelson interferometer and the Mach-Zender interferometer. Both of the configurations are based on the same principle: one branch of the interferome-

ter, called reference will be in free space while the other branch will travel through the vacuum vessel, travelling the same distance until maximum constructive interference. In presence of plasma, the path length between the two branches will be different, causing an interference pattern which can be directly linked to the refraction index and therefore to the density (see Fig 3).

$$\Delta\phi = \frac{2\pi}{\lambda}\int_{z_1}^{z_2}(1-(1-\frac{n_e(z)}{n_c})^{\frac{1}{2}})dz \tag{21}$$

with the $\Delta\phi$ phase difference directly linked to the line integral of the index of refraction $n_e(z)$ on a portion of plasma placed between z_2 and z_1 .

A single chord measurement is sufficient for a general density control diagnostic in many plasma fusion experiments, whereas a multiple chord experiment uses the many points of view of the plasma to evaluate its density profile. Vibration and mechanical motion of the system, that induce an error in the phase measurement, can be overcome with the two-color interferometry method, where two beams with slightly different frequencies propagate in the plasma and the difference between their index of refraction eliminate the identical vibration contibrute in the measurement leaving only the plasma contribute.

2.2.2 *Polarimetry*

A plasma becomes slightly birefringent in presence of magnetic field. This effect can be used to inspect certain properties of the plasma, such as the density and the magnetic field strength itself. Two are the observable physical effects that can be used

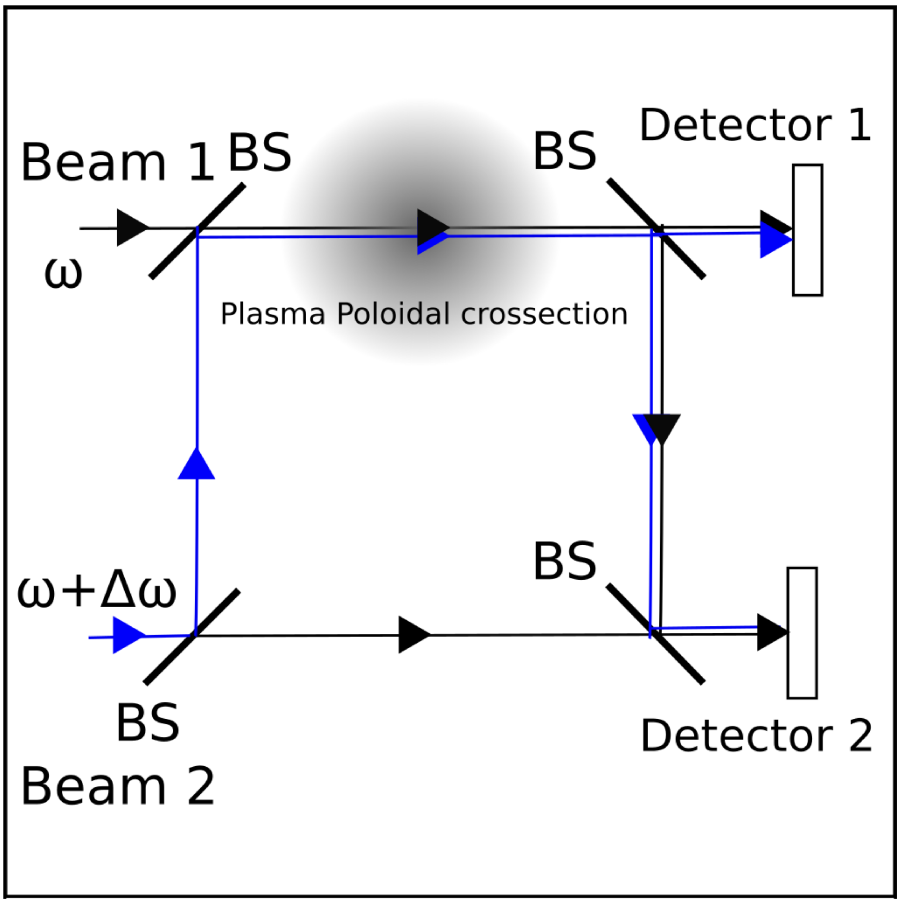

Figure 3: Principle of a heterodyne scheme for simultaneous Faraday rotation and interferometry measurements in Tokamaks. The black line represents the reference branch, in which the laser that travel in air. The other branch is represented by the blue line where the laser beam travels inside the plasma. There will be intereference on detector 1 and 2 that can be detected and from that is possible to derive the phase delay induced by the plasma.

to explore the plasma's properties: Faraday rotation and Cotton-Mouton effects which we will briefly proceed to outline.

A Faraday rotation is a birefringence effect induced by the magnetic field in which a linearly polarised wave propagating in a magnetised plasma will rotate around its plane of polarisation.

The Cotton-Mouton effect alters the ellipticity of the wave. Both of these effects are insensitive to vibration and independent to path length, depending only on changes in the polarisation.

The angle of Faraday rotation of a linearly polarised monochromatic wave propagating through a distance L inside the plasma when $\frac{n_e}{n_c} << 1$ with n_c the cut off frequency density and L the ray path in the Plasma is as follows:

$$\alpha_{Faraday} = \frac{e}{2m_e c} \int_L \frac{1}{n_c} n_e B \cdot dl \tag{22}$$

2.2.3 *Reflectometry*

Reflectometry is a very attractive method due to its multipurpose diagnostic relevance to the measurement of density profiles and density fluctuations with only a single view of the plasma. The working principle of the diagnostic is based on radar technology: a wave with a fixed frequency propagates in the plasma until its density reaches the cut-off density value upon which the wave is reflected. Mathematically this translates into the plasma's index of refraction becoming purely imaginary. When the wave returns to the point of origin, it carries a phase delay which is conceptually equivalent to the time delay of a radar echo [6].

As shown in equation (23) the point of reflection x_c depend on the difference of phase delay ϕ in respect to the point a , with $\omega_c = 2\pi f_c$ and f_c the cut off frequency [6].

$$\phi = \frac{2\omega}{c} \int_{x_c}^{a} N dx - \frac{\pi}{2} \tag{23}$$

$$x_c(\omega_c) = a - \frac{c}{\pi} \int_0^{\infty} \frac{d\phi}{d\omega} \frac{d\omega}{(\omega_c^2 - \omega^2)^{\frac{1}{2}}} \tag{24}$$

The signal measured as a sum of reflections can be difficult to interpret for the various fictitious reflections that can be induced by fluctuations, plasma gradients and Vessel reflections. The basis of reflectometry theory is the propagation in O-Mode and X mode where the former is determined by the plasma frequency and recovered by Abel inversion [6] , the latter is dependent also on the gyrokinetic frequency and determined numerically. A finite density gradient is required in O mode while a flat, or null density gradient is present in X mode. Due to this characteristic, a wide range of frequencies are needed to obtain a full density profile in X mode, resulting in a better localisation than O mode. The configurations for reflectometry are illustrated below [26] [27]:

- Frequencies Modulation - Continuous Wave (FM-CW): Linear frequency sweep between two frequencies of a continuous wave. In this configuration, pulse reflection is measured with the time of flight, τ_f. This is a measurement of the beating between the reference signal and the wave after it has been reflected into the plasma is done by measuring the fringe frequency between the two. The main limitation of this configuration comes from long probing intervals, caused by the finite millisecond sweep time of frequency, during which turbulence inside the plasma could interfere with the measurement.

To overcome turbulence the measurements are taken using a millisecond time scale, inferior to the turbulence temporal life, freezing the turbulence. By averaging the measurements, the density profile is obtained.

- Amplitude Modulation: The amplitude modulation (AM) of the phase difference of two waves are seen as a way to overcome the slow step of frequencies modulation system. The time delay is also measured as a phase shift between closed separate frequencies launched simultaneously. The main advantages of this configuration is the simultaneous launching of the whole spectrum even if the phase delta is smaller than the frequencies modulation system.

- Pulse radar: Derived from applications of radar technology, this involves a Fourier method, for which the delay time of round trip pulse is measured, instead of the phase difference. Using a Fourier transform, a pulse can be decomposed into discrete frequency components each with a particular amplitude and phase, and can be considered as monochromatic wave with each a distinct amplitude and phase. An inverse Fourier transform therefore provides the same information as can be obtained by a direct pulse measurement. In a common pulse radar system, a set of discrete waves are launched towards the plasma, contained within total bandwidth $\Delta\nu$. The spatial resolution required to discern the pulse radiation, is a [28] pulse of 70 ps, therefore a time resolution of the order of a picosecond is needed. As the snapshot-like measurement, deals with the static plasma, the determination of the density profile is not perturbed by temporal fluctuations of the density. The reflection from the plasma can be distinguished from the spurious reflections. The major limit of the Pulse radar technique is a SNR ratio lower

than the corresponding one for a frequencies modulation system, implying that the hardware technology has to be improved to be of use in practical application.

- Ultrashort Pulse Reflectometry: A pulse of picosecond encompasses all the frequency spectrum required in reflectometry measurement (around 100-300 GHZ). The measurement consists in recording the time delays of all the frequencies. It has the same advantages of a conventional pulse radar, but an additional advantage is that all the frequencies can be launched simultaneously. The major limitation of this type of diagnostic are the low SNR (Signal to Noise Ratio), with the demand of Pulses with a high energy peak amplitude because the power is spread over all frequencies. Another issue is that the detection system have to provide enough spatial resolution to distinguish the pulse with enough frequencies resolution (on the order of dozens of GHz).

2.3 THZ PLASMA DIAGNOSTIC APPLICATIONS

From equation (15) and remembering the relations for plasma frequencies and cyclotron frequencies:

$$\omega_p = \sqrt{\frac{n_e e^2}{\epsilon_0 m}}, \omega_{ce} = \frac{eB}{m} \tag{25}$$

where n_e is the plasma density, e and m the electron charge and mass, ϵ_0 the vacuum permittivity and B the magnetic field. To notice that in the text is used, following an habit in the plasma community the term plasma frequency with the term ω_p even if is actually a "pulsation" expressed in rad/s . It is possible to derive the ordinary and extraordinary index of reflection, and from that some of the useful quantities needed to

characterize the propagation of an EMW inside the plasma (see Fig 4).

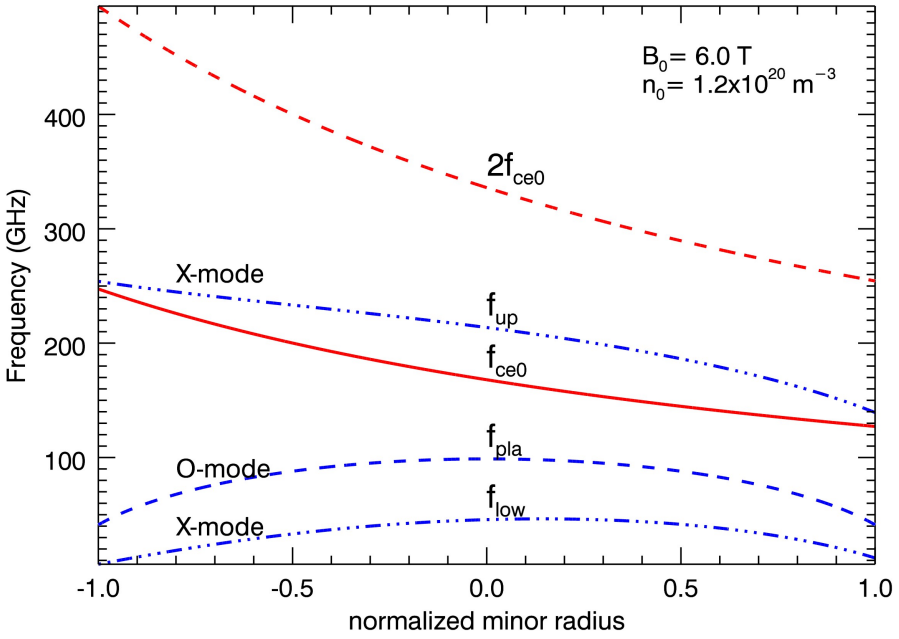

Figure 4: Accessibility of EMW in a plasma, with a visual, expressed in Hz, of the plasma frequency f_{pe}, the cut-off frequencies of upper and lower hybrid f_{up}, f_{low} and the cyclotron frequency f_{ce} [5].

Application as diagnostic for ftu have been studied in [29] [30] for the diagnostic can be derived using the parameter of FTU (Frascati Tokamak Upgrade) machine, which has minor radius 0.31 m, maximum magnetic field of 8. The X-mode provides good accessibility (> 50 %) in most plasma regimes and especially at low density in the 0.1-1 THz range as shown in figure 5, with the *accessibility* defined as the decimal fraction of the plasma radius which can be probed by the electro magnetic beam before encountering a cutoff layer [1].

By resolving the phase shift of selected individual components of the whole THz spectrum, the radial density profile can be obtained by Abel inversion [28],[31].

Interferometry in tokamak using THz-TDS can be used in conjunction with polarimetry. The THz-TDS scheme with po-

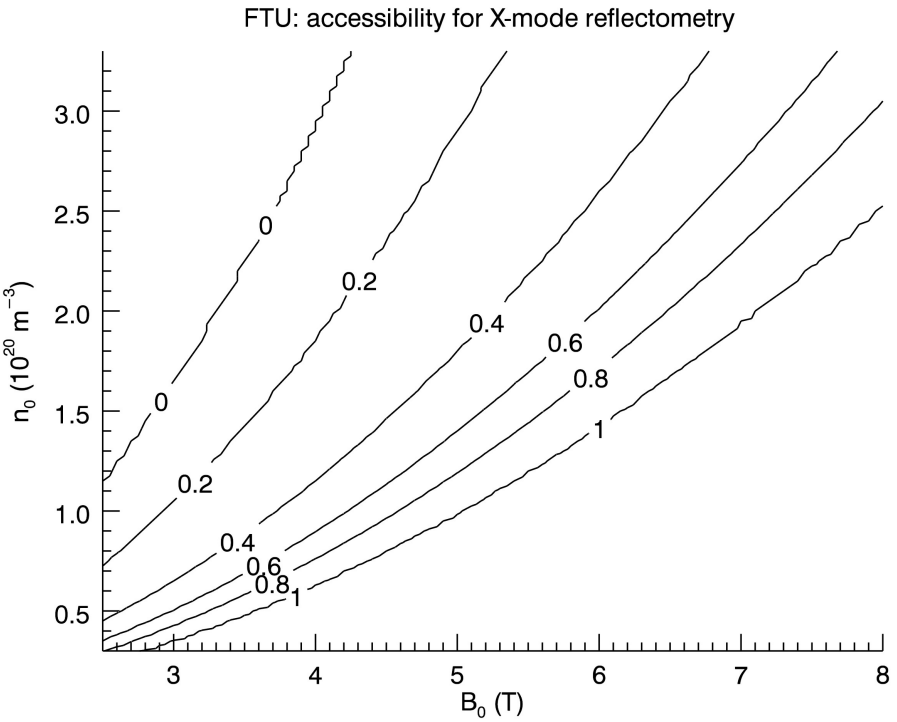

Figure 5: X-mode reflectometry: parametric curves of equal accessibility of FTU radius vs. peak density n_0 and magnetic field B_0. In the central region of the graphic: $f_L=\frac{\omega_L}{2\pi}$=80 GHz, f_R=220 GHz, f_p=130 GHz [32].

larisation resolving detector would provide a straightforward implementation of the combined measurement where the same optical setup can be simultaneously used for the two diagnostics, without need for extra components. A direct measurement of the plasma refractive index can be obtained by using several spectral components of the THz beam, where the low range < 300 GHz can be used for reflectometry and the high range > 300 GHz to 1-2 THz can be used for Interferometry. In this way a direct measurement of the plasma refractive index can be obtained, and hence the density can be measured directly. This is analogous to a multicolor interferometry set-up. The different components are used to increase the calibration accuracy of the diagnostics. The applicability of THz-TDS interferometry for FTU is illustrated in Fig. 6. Note that the line integrated plasma density can be derived from the difference of the phase shift of the electric field at different frequencies.

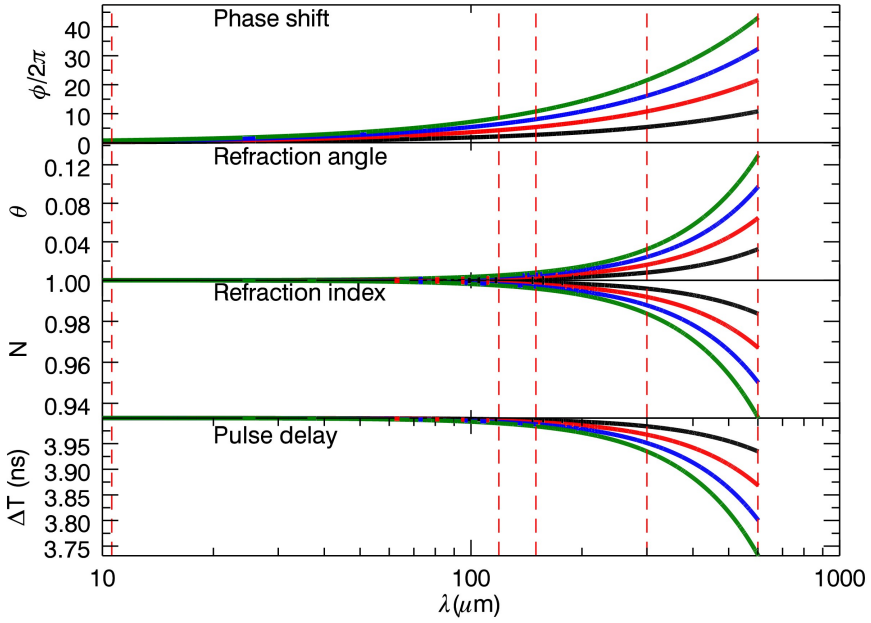

Figure 6: Simulation of relevant properties of EMW propagating trough FTU plasmas,minor radius a=0.3, as a function of wavelength, assuming a parabolic density profile and for different values of the peak electron density in $10^{20} m^{-3}$ units:n_{e0}=1 black, n_{e0}= red, n_{e0}=3 blue and n_{e0}=4 green. The vertical dashed lines mark the wavelength of the CO2(10.5µm) and DCN (119µm) lasers used for traditional interferometry. The range from 150 µm to 600 µm continuously covered by THz pulses is also indicated. [32]

3

THZ-TDS INSTRUMENTATION

3.1 INTRODUCTION

A THz-TDS set-up utilises an electro magnetic pulse to measure the frequency spectrum and other optical properties of a sample dielectric function. Three configurations are frequently used: transmission set-up, scattering set-up and reflection set-up [15]. In the transmission set-up, the pulse propagates through a strong, but not fully opaque absorber; in the scattering set-up, the pulse is displaced in all direction; and in the reflection set-up the pulse is reflected by a medium, usually a strong absorber.

The three set-ups require a reference background measurement, taken without the medium, as a comparison with the pulse that has interacted with the sample.

A typical THz-TDS system is composed by a pump and probe system as shown in Figure 7.

Following the set up in our laboratory in Frascati the scheme can be described as follow: A seed laser Nd:YAG Verdi system 532 nm, power rating 10W is coupled as a pump to a Mira 800 nm mode-locked laser. The device generates a 170 fs long pulse that is separated into two branches by a beamsplitter, according to 90/10 intensity ratio. Of the two, the high intensity branch is destined for the emitter, and is referred to as pump branch. Conversely, the low intensity branch is directed at the detector and named probe branch. The former generates the THz

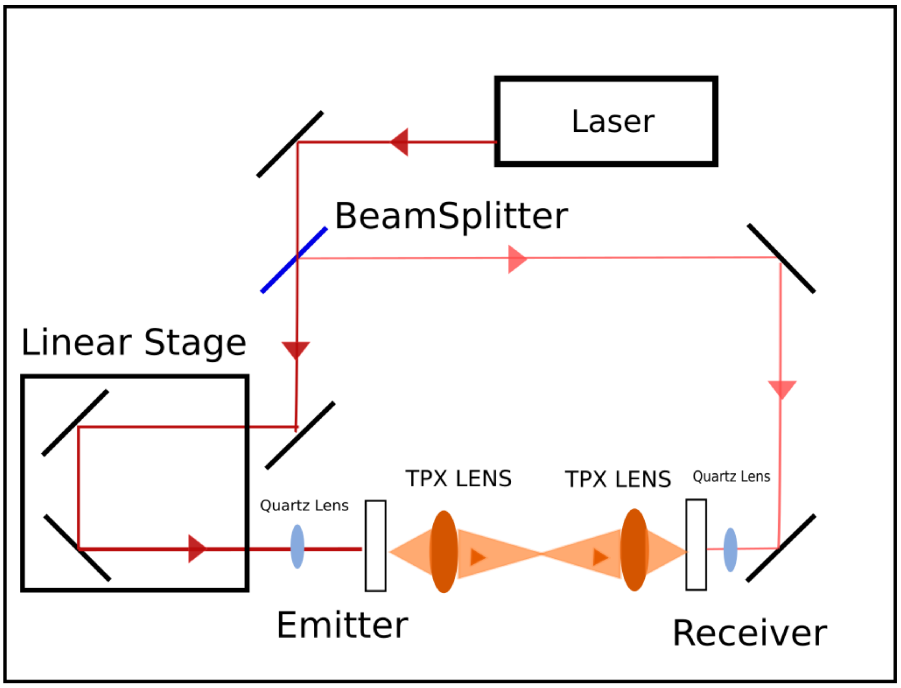

Figure 7: THz-TDS set up. A pulse generated from the fs laser source, with wavelenght λ_0=800 nm, is divided in two branches by a beam splitter. One branch go through a delay stage and is focalised by a quartz lens to photo excite a GaS semiconductor slab that is the source of the THz pulse. The other branch is focalised by a quartz lens to photo excite another semiconductor slab that is used as detection system. Two TPX lens with focal length of 85 mm are used to focussed the THz pulse on emitter and detector.

pulse, the latter for sampling the THz electric field. The pump branch travels through an optical system mounted on a linear translation stage, successively focused by a quartz lens onto the semiconductor emitter. The probe branch is focused by another quartz lens onto the detection element. The linear stage introduces an optical path difference (PD) between the source and the detector. Zero path difference (ZPD) results in activation of the detector at the beginning of the THz pulse. Increasing the PD causes the detector to be activated at a different stage of the pulse. By measuring the distance of the activation position from the beginning of the pulse, the electric field of the pulse can be scanned, sampling the THz pulse in both amplitude and phase. A lock-in amplifier is used to increase the sensitivity in order to acquire a time domain pulse, which carries phase information. From this pulse, the spectral information is easily derived using a fast Fourier transformation.

3.2 CHARACTERISTICS OF A THZ-TDS SYSTEM

A THz-TDS set-up is a wideband spectrometer with up to 1 GHz resolution. The general properties of this instrument will be outlined in the first part of this chapter, all derived from [15].

BANDWIDTH The bandwidth of a THz-TDs system is mainly conditioned by two factors: the source bandwidth emission and the detector response. Taking as a reference point the commercial THz-TDs spectrometer, which functions with the technology of the photoconductive antenna, it is shown that the achievable bandwidth is 0.1 - 6 THz. In the plasma diagnostics research field, new generation devices, performing electro-optical sampling and functions of air plasma-antennas, can successfully generate pulses with bandwidth usually in the

15 THz range, sometimes reaching 200 THz [20]. The principal drawback for systems employing ultra wide emission sources is their technological limitation: present-day detectors are not equipped with wide enough detection ranges. The one used in this project showed gaps in its detected spectrum, due to phonon modes. [20].

FREQUENCY RESOLUTION The signal $S_{meas}(\omega)$ acquired by the THz detector is the convolution between the temporal width of the scanning window T_{wind} and the signal itself.

$$S_{meas}(\omega) = \frac{1}{2\pi}\int_{-\infty}^{\infty} G(\tau, T_{wind}) i_{det}(\tau) e^{-j\omega\tau} d\tau \tag{26}$$

Where i_{det} is the current generated by the detector, and $G(\tau, T_{wind})$ is a rectangle function equal to 1 $<\tau<$T and 0 everywhere else. From Fourier Transform theory, the measured signal can be described as:

$$S_{meas}(\omega) = T_{wind} S(\omega) \wedge sinc(\frac{T_{wind}}{2}) \tag{27}$$

The experimental frequency resolution is equal to Δ f = $1/T_{wind}$, that is to say: using a 5 ps time window, equivalent to 5 cm on a linear scanning stage, a frequency resolution of 3 GHz is obtained. Perfect optical alignment, which is difficult to obtain for optical path longer than 5 cm, is a necessary requirement to achieve resolution in the finer frequency range.

Another way to obtain better resolution is to utilize ASOPS (Asynchronous Optical Sampling System), a system where two mode-locked lasers carrying different pulse repetition rates are manipulated to give a temporally varying delay between the two pulses, reaching frequency resolutions as low as 1 GHz, advantageous due to kHz scanning rates [33].

SPATIAL RESOLUTION The spatial resolution in a THz-TDS system depends on the diffraction limit of the focused THz beam. With 0.6-6THz corresponding to wavelength range of 0.05-3 mm, and with a lens of Numerical Aperture (NA) of one, the diameter of the limiting spot varies approximately from 0.12 to 7.5 mm.

SIGNAL TO NOISE RATIO Let's define SNR and DR dynamic parameters to describe TDS performances:

$$SNR(\omega) = \frac{S(\omega)}{\sigma(\omega)} \text{ and } DR = \frac{S(\omega)}{S_{min}(\omega)} \tag{28}$$

where $S(\omega)$ is the THz amplitude at angular frequency ω, $\sigma(\omega)$ is its standard deviation and $S_{min}(\omega)$ is the minimum measurable signal at ω. If $\sigma(\omega)$ is signal independent, then SNR and DR are equal. $\sigma(\omega)$ standard deviation arise from the noise of the system and depends principally on Relative Noise Intensity (RNI), dependent on the flutuation of power of the laser source, shot Noise of the Detector, dependent on the discrete nature of the electric charge and Johnson Noise in the detection, or the electric noise originated by the Brownian motion of the charges in the device and depends on its resistivity and temperature [21].

In the case of a photoconductive emitter, the power of the emission is linearly proportional to the power of the exciting laser, so that the RNI of emitter and laser are directly linked. So the SNR of the system is dependent on the laser power stability. The remaining source of the noise depends on the physical characteristics of the detector (semiconductor properties and excitation conditions). It is interesting to note that beyond 500 GHz the relevant source of noise is the thermal noise, because the THz signal level decreases rapidly decreasing the RNI. The

total deviation can be expressed as the sum of the individual contribution, as:

$$\sigma_S^2 = x^2\sigma_E^2 + 2qs\Delta f + \sigma_D^2 (x = \tau \text{ or } \rho) \tag{29}$$

Where σ_E is the noise from the emitter, s is the detected THz signal magnitude, q the charge of the carriers and Δf the detection bandwidth,σ_d the thermal noise from the electronic detection, the third term is dependent on the shot noise of the detector and x representing the τ trasmission or ρ reflection coefficients.

3.3 THE BASIS OF THZ-TDS SPECTROMETRY

3.3.1 *Transmission*

- Measurement of the THz pulses, S_{smp} (t) and S_{ref} (t) are obtained respectively with and without the sample positioned between the emitter and the receiver.
- Calculation of the complex transmission of the sample is carried out by calculating the ratio of the complex FFT spectra of the temporal waveforms S_{smp} (t) and S_{ref} (t) to obtain the transmission function $H(\omega) = \frac{FFT(S_{smp}(\omega))}{FFT((S_{ref}(\omega))}$.
- From the experimental transmission function it is possible to extract the index of refraction n and extinction coefficient k, utilising theoretical model [34] of the transmission property of the media .

The reference and signal, from which the phases of the spectrum, are measured as a function of the delay introduced by the mechanical stage and so these must absolutely be recorded

with the same time origin in order to extract the index of refraction from the phase delay between the two signals.

The complex index of refraction of the sample is measured directly from the transmission function: whilst easily obtainable in the most common case of the thick slab, the thin slab case is more complex, as it presents a secondary reflection interfering with the first in the same time window. Using the thick slab approximation it is possible to derive the theoretical trasmission T_{th}:

$$T_{th}(\omega) = te^{i\phi_t} 4 \frac{\tilde{n}}{(\tilde{n}+1)^2} exp(-i(\tilde{n}-1)\frac{\omega}{c}d) FP(\omega) \tag{30}$$

where ϕ_t is the phase componente of the trasmitted element and t is the fresnel trasmission coefficent, n the index of refraction of the element, d the thickness of the element and $FP(\omega)$, the Fabry Perot effect of the element is as follows:

$$FP(\omega) = \frac{1}{1 - (\frac{\tilde{n}-1}{\tilde{n}+1})^2 exp(-2i\tilde{n}\frac{\omega}{c}d)} \tag{31}$$

From these elements it is possible to derive the thickness of the slab for a known $\tilde{n}$, or conversely extract the refraction index for a known slab thickness. In presence of echo and reflection, it is also possible to directly extrapolate the thickness of the element. The index of refraction from the reflection measurement can be obtained with a experimental procedure similar to the one used in the transmission measurement. Here, the reference signal is obtained by putting a perfect reflecting mirror in the position over which the sample is held. In the case of a strong absorber there will be no rebound reflections inside the media, the theoretical reflection R_{th} can be described as:

$$R_{th}(\omega) = re^{i\phi_r} = \frac{\tilde{n}-1}{\tilde{n}+1} \tag{32}$$

And from this relation it is possible to derive the index of refraction n and the extiction ratio k directly linked to r, the reflected modulus, and ϕ, the phase (or argument) of the reflection [15].

3.3.2 *THz emitters and detectors*

The emitter used in these experiments was often a photoconductive type of antenna. A photoconductive antenna consists in a semiconductor substrate supporting two stripes of gold, separated by a suitable gap and in the one used during the experimentations usualy between 400 μ and 1mm gap, depending on the semiconducor and required THz range. The detection devices used were both photoconductive antennas and electro-optical sampling detection systems.

3.3.3 *Emitters*

THz generation [35] derives from the conversion of an IR pulse in the range from a few fs to ps, which have a spectral bandwidth in the THz range using a converting element, like a GaAs semiconductor or a non linear optical crystal as show in Fig 8. THz detection relies on the properties of the medium to detect the he THz electrical field: by varying the linear stage, it is possible to sample the temporal propagation of the Electric field.

A THz pulse is generated when a voltage is applied and a ultrashort Laser pulse (fs) hits the gap between the two electrodes. A square signal is used to modulate the signal and give a reference trigger to the lock-in. The fs pulse acts as a switch for the semiconductor. To convert photon energy of the IR pulse in a THz Single-Cycle, two phenomena are exploited: the Surface emission and the Photo-Dember effect [35]. The pulse gener-

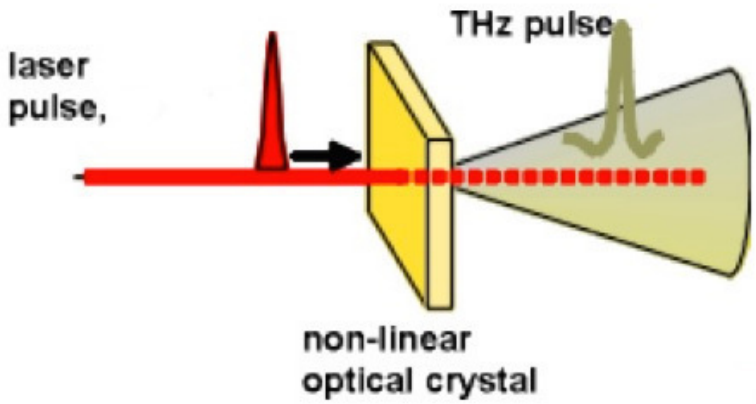

Figure 8: THz generation scheme.

ated from the above set-up carries a linear polarisation, which is parallel to the biased field. When the photon energy is absorbed, free carriers are generated inside the semiconductor. Inducing an external electric field these carriers can be made to oscillate thanks to which a THz front is produced, a similar process to that of the dipole antenna. The variation of the photocurrent with time, due to the external field, can be approximated as:

$$E_{THz} = \frac{dJ}{dt} = q_{e,h}\frac{dN_c}{dt}v_{e,h} + q_{e,h}N_c\frac{dv_{e,h}}{dt} \tag{33}$$

where N_c is the carrier density, $v_{e,h}$ the carrier velocity and $q_{e,h}$ their charge. The energy of the THz pulse originates from the electric energy stored across the gap, but is limited by the pulse energy of excitation, where after a certain energy value there are no variations in the THz emission intensity. The energy value depends on the substrate used.

The device operates when the biased field value V_{ext} is less than the value for dielectric breakdown field of the substrate used as semiconductor, i.e. $V_{ext} = 4 \cdot 10^5$ V/cm in GaAs. There

are two limiting factors for the bias voltage intensity: instantaneous breakdown and thermal induced breakdown. Too strong fields will induce an electron avalanche which will cause instantaneous breakdown. Thermal induced breakdown is caused by the heating of the substrate which originates from both the excitation laser intensity and the biased voltage, provoking a decrease in the global electric resistance, which in turn will induce a high photocurrent flow. This can lead to a breakdown after a current flow period ranging from a few seconds to minutes.

3.3.4 *Detectors*

3.3.4.1 *Photoconductive detection*

A photoconductive antenna can also function as a THz detector when irradiateted with a IR pulse. The major difference from its capacity as an emitter, is that the two electrodes of the detector are not externally biased, but connected to a current sensor. The Fermi level of a surface state may be different than in the bulk material. In GaAs n-type semiconductors, the Fermi level is closer to the conduction band, thus higher than the Fermi level of the surface state which is closer to the center of the gap. The surface electric field drives free electrons drifting toward the inside of the bulk material. As result, the free electron density in the surface field layer is much lower than within the bulk material. The surface field layer is hereby named the depletion layer.

The THz electric field between the gap inside the electrode induces a measurable current. With the delaying stage all the pulse can be sampled.

$$j(t) = \frac{1}{T}\int_0^T E(t)\sigma(t+\tau)dt \tag{34}$$

if $\sigma(t+\tau) = e\mu N_c$ is comparable to a delta function , the detector is able to detect the same pulse shape as the THz pulse.

3.3.4.2 *Electro-optical Sampling*

Electro-optical sampling (EO sampling) is a process that aims to detect incoming THz pulse by exploiting the frequency mixing property of a nonlinear medium, that presents a birefringent variation caused by an incoming electric field. A linearly polarised probe beam, that travels collinearly to the THz field inside a EO crystal will have its phase modulated by the refractive index change induced by the electric field of the THz pulse, inducing a variation in its polarization state. The polarisation can be detected converting its change into an intensity change, by means of an optical analyser. Using a Wollaston prism the probe beam can be separated into its two linear polarisation states (horizontal and vertical). By measuring the intensity of each separated beam, the initial polarisation state can be deduced.

The phase delay $\Delta\varphi$ can be calculated according to variations in the refractive index, with the processes assumed to be phase matched and is shown in the following equation:

The phase delay of the crystal called Γ is:

$$\Gamma = \frac{\pi d n_o \gamma_{41} E}{\lambda} \sqrt{1 + 3\sin^2\phi} = d\pi \frac{E}{E_\pi} \tag{35}$$

In the case of GaP crystal and 110 crystal orientation,d the crystal thickness, γ_{41} the intrinsic EO coefficent of the crystal and the EO coefficient of certain EO crystals can be represented by half wave field , E_π^{GaP}=161 kV/cm was used in this thesis, ϕ the angle of the crystal optical axis in respect of the plane of polarization of the incoming Electric field. [36].

To obtain a measurement of the phase delay there are two most commonly used methods: cross and balanced measure-

ments. The latter was chosen, for it yields higher signal and directly measures the THz Electric field.

A linearly polarised probe beam is modified to obtain elliptical polarisation through the EO process. A quarter-wave plate is used to balance PDS the polarisation of the probe beam. A Wollaston beam is used to split the biased probe beam into the two perpendicular polarized components between the two polarisation components. A pair of balanced photodetectors is used to measure the difference between the two polarisations. When no THz field is applied, the s and p components will have the same intensity, and the detector will emit no signal. A non-zero THz electric field changes the polarisation of the probed beam, generating a measurable signal in the detector. In case of an X polarised input beam the signal is as follows:

$$S = I_0(sin2\phi \ sin\tfrac{\Gamma}{2})^2 \tag{36}$$

with S the signal, I_0 the IR laser intesity, ϕ the angle between the long axis of the ellipsoid of the EO crystal and the IR polarization and Γ is the phase delay induced by the EO crystal.

The three factors that limit the bandwidth of THz radiation in EO sampling are the pulse duration of the excitation laser pulse, the phase matching condition and the longitudinal optical (LO) phonon absorption [37]. A laser pulse can generate a THz pulse with a bandwidth of the order of twice that of the laser pulse. Therefore with modern ultrafast lasers the bandwidth should exceed 100 THz. The limiting factor is the phase matching of the material, that convoy only a fraction of the THz bandwidth. One way to distance the effective phase matching is to decrease the thickness of the material ad so the coherence lenght, whilst considering that this will increase the mechanical weakness and low optical damage threshold.

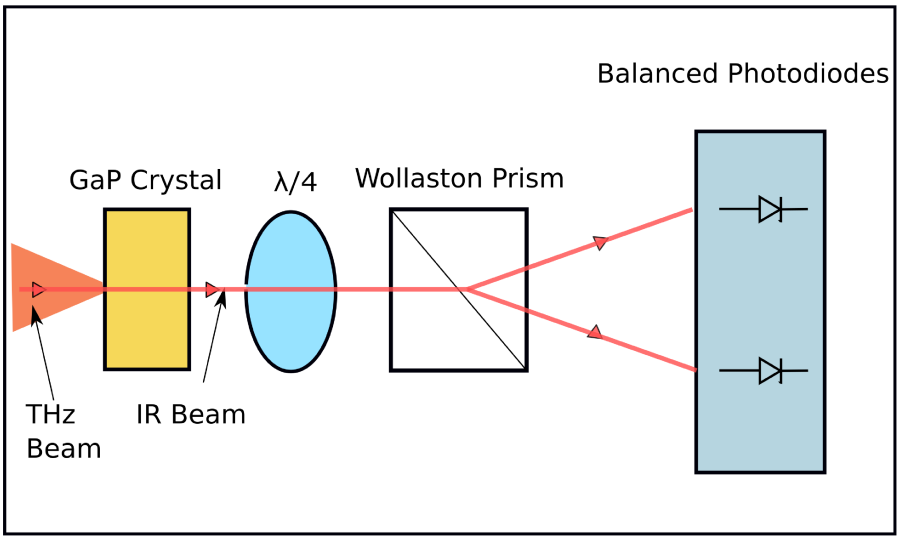

Figure 9: Scheme of an electro-optical detection set up. A fs laser pulse shines collinearly through the THz pulse through a non linear crystal. Then this polarisation can be controlled by a quarter wave plate (λ/4) and then is divided in its two polarization states (H,V) by a Wollaston Prism and the two beam (separated by a fixed angle) are detected by a pair of balanced photodiodes.

3.3.5 *Mode-locking Laser*

Mode-locking technique is a unique second order laser technique, used to produce coherent laser pulses in the range of picoseconds (10^{-12}) or femtoseconds (10^{-15}). The basis of the technique is to induce a fixed phase relationship between the longitudinal modes of the laser resonant cavity. Constructive interference between these modes allows the laser light to be produced as a train of pulses. The laser is then said to be 'phase-locked' or 'mode-locked' as shown in fig 10.

A keystone feature to the generation of ultra-short pulses is the laser cavity with its longitudinal and transverse modes. Mode-locked operation requires a well-defined mode structure. Transverse mode structure enables amplitude noise, therefore a typical laser cavity is built to support a large number of longitudinal modes, whilst only operating at a single TEM_{00} trans-

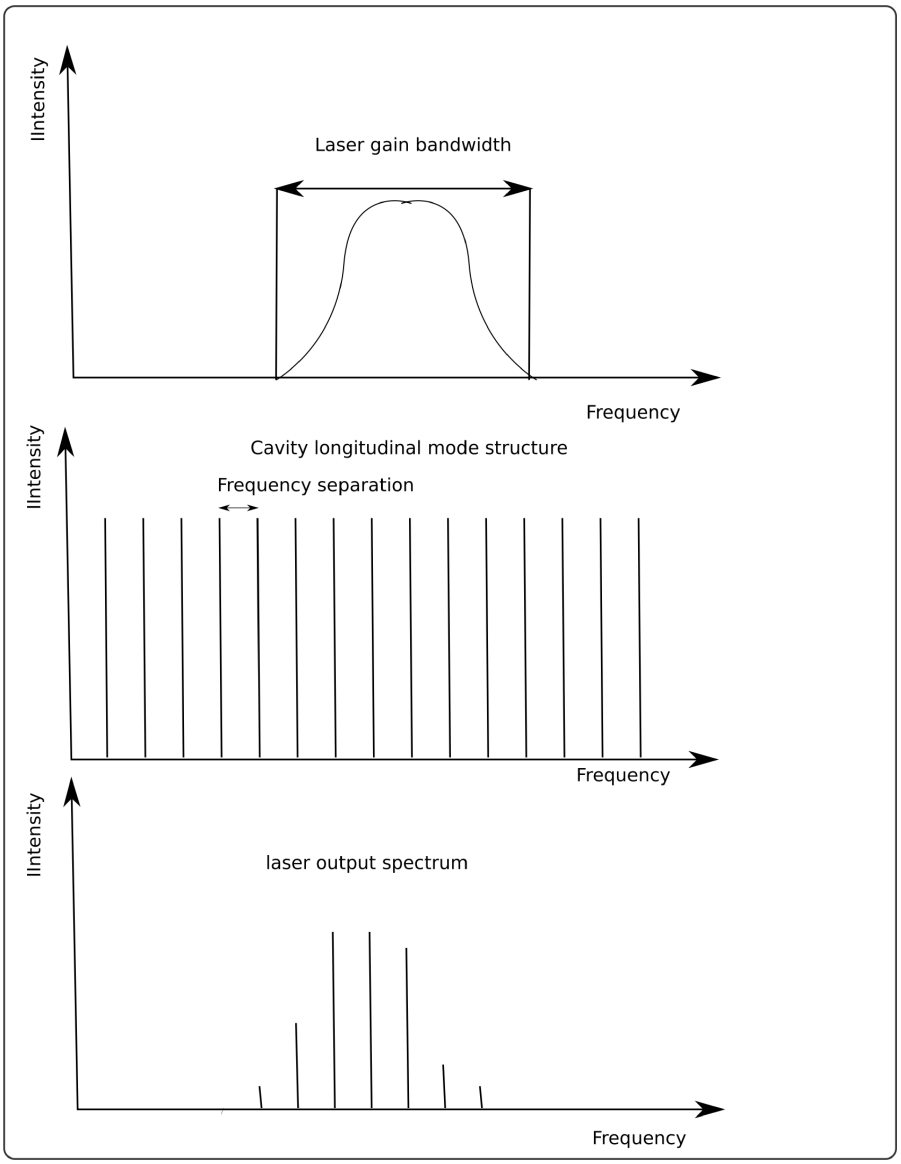

Figure 10: The scheme of generation of a Mode Locked laser. It is shown how part of the combed frequency laser structure inside the cavity of the laser is selected by the mode locking in the laser output in order to generate a short laser pulse [38].

verse mode. In absence of transverse mode structure, we can assume that the laser can operate on any longitudinal modes of index m, with frequencies $\nu_m = \frac{mc}{2\nu(\nu_m)L}$. $\nu(\nu_m)$ is the effective average optical path lenght at ν_m frequency of the geometrical cavity length L. [39]

The electric field of a laser that oscillates on a number of adjacent longitudinal mode m of frequency $\omega_m = \omega_l + 2\pi m\Delta$, with $\Delta = \nu_{m+1} - \nu_m$ the mode spacing and equal field amplitude E_0 can be written as the sum of all the singular modes each with its random phase. The laser field is a repeating pattern with a periodicity equal to the cavity round-trip time $\tau_{RT} = \frac{1}{\Delta}$.

For a random phase, the average of the laser emission is the sum of the intensity of the individual modes. For a fixed equal phase (forced externally, and so mode-locked) it follows that in the time domain, all of the waves will constructively interfere in one point, resulting in a train of intense pulse of light, separated by the cavity round-trip time and of duration of $\tau \approx \frac{1}{\Delta M}$.

One of the most common and used laser sources for a fs pulse generation is a Ti-Sapphire Laser [39], featuring notable specifications such as the largest bandwidth, a large nonlinear index, thermal and optical properties.

A typical configuration, illustrated in Fig 11 is made of a frequency doubled Nd:YAG laser with power from 5 to 10 W to excite the nonlinear medium constituted by the Ti-Sapphire rod. This last element is contained inside two cavity mirrors, as for typical laser source and some dispersive elements (in our case two prisms). To achieve mode-locking, a pulse source seed is needed, as well as a gain method that can be active or passive, with the dispersive elements for reducing the pulse width.

Diverse techniques of pulse generation have been developed, but they are all based on the working mechanism of the opti-

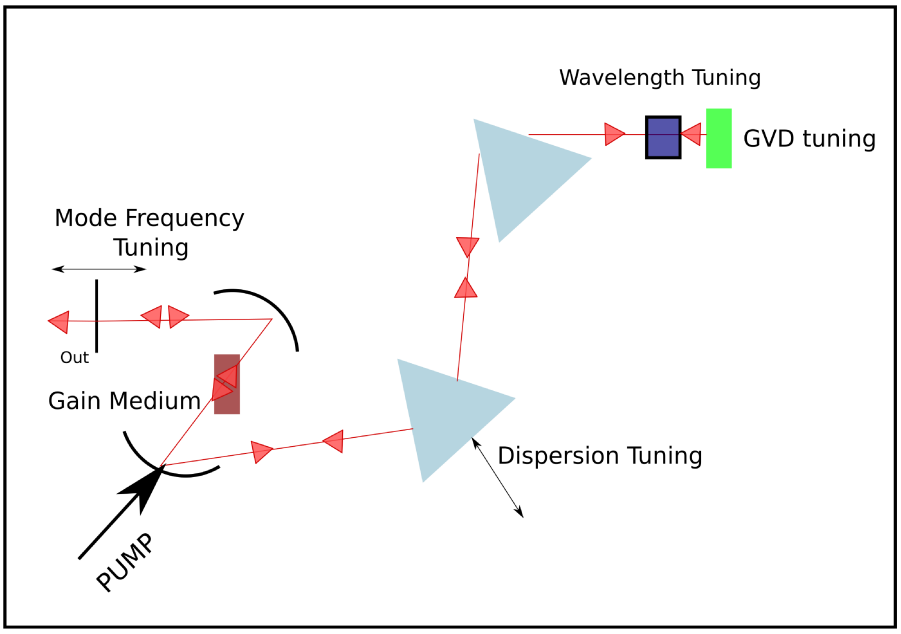

Figure 11: Typical Ti:Sapphire laser cavity consisting (from the right) of an end mirror, an aperture, a prism pair, folding mirrors at both sides of the laser crystal and an output coupler. The various adjustements that are possible on this laser are discussed in [39].

cal shutter, where the beam is transmitted for the desired time intervals, then amplified.

The shutter effect can be achieved by means of a passive element with a certain mechanism, which is outlined below for the MIRA 900.

In the Mira 900 coherent laser the passive element [38] is a saturable absorber system, in the place of more commonly used dyes or liquid that do not have to be removed. The system operates independently of the wavelength and can be adjusted for various incoming power levels.

During the continuous-wave (CW) operations within the Mira cavity, the diameter of the beam is larger that the pulsed beam diameter. A simple slit is adjusted to let pass the pulsed beam, and interrupt the CW at the edges of the beam trasverse diameter, in fact removing the CW signal.

Using the Kerr-lens effect it is possible to change the diameter of the beam. When high power light interacts with the absorber element, its index of refraction n changes, proportionally to the light intensity. For a circular beam, which presents higher intensity in the center than in the outer edge, that the variation in the index of refraction n will be different. This is analogous to an optical lens, where the center has an optical path larger than the edge, so that the light is focused. This effect is observed only when the pulse is mode-locked, carrying a high power density with respect to CW, so a starting mechanism has to be defined. Changing the cavity length at the proper speed, high power fluctuations can be induced. Once the instantaneous power in one of these fluctuations becomes sufficiently high, a Kerr lens is formed and the beam is narrowed and can pass unattenuated through the slit. This pulse will become amplified and become the dominant pulse which will form the mode-locked output. The length of the cavity is changed by tipping the angle of a glass plate through which the beam must travel, changing the optical path.

3.3.6 *High Voltage Amplifier*

An inverter amplifier based on the PA98, a high power operational amplifier from APEX microtechnology is used to induce the bias voltage on the emitter. This circuit provides an amplification of 14.7 times (23.3dB) and a maximum output of 300 V_{pp} and 100 mA [40].

3.3.7 *Lock-in amplifier*

Lock-in amplifiers are used in experiments that require to extract a small (even lower than the order of nA) electric signal

coming from the operational hardware, dominated by noise coming from different sources. The signal can be described as

$$V_{signal} = V_0 + V_{noise} \tag{37}$$

with V_0 the original signal and V_{noise} the noise signal. There are many type of noises that can derive from the signal to measure itself or from the instrumentation used. Examples are white noise, Johnson , $1/f$ noise [21]. Their common trait is that they are not coherent with each other, and can be summed as the square root of all the noise sources. If part of the signal is composed of a repetitive element , which may be inherent in the phenomenon or imposed by the experiment, e.g. if it is chopped at a fixed frequency, it is possible to use a a lock-in. The input signal is amplified and then filtered from the noise. Feeding the lock-in "lock" with the frequency of the repetitive phenomenon, it will lock on input signal and extract that particular frequency (within the physical limits of the instrument, with an extremely small bandwidth i.e.3-3dB , separating the signal from the output of sync component of the noise.

3.3.8 *Fiber Optics based THz spectrometers*

It is well known that diagnostic access to Tokamaks is extremely difficult, due to the complex electrical and mechanical structure of the device, the strict vacuum requirements and the need of screening outgoing neutrons and plasma radiation. These issues will become more relevant going towards next generation machines, not to mention the reactors. In this view THz-TDS offers a unique capability of performing wide span diagnostic measurements by reaching the plasma with relatively small sensors, to be accommodated easily behind suitable vacuum windows. In addition, the IR laser radiation can be guided to the

THz generation and detection devices by single mode optical fibers for considerable lengths (>10 m). This will of course pose the issue of Group Velocity Delay (GVD) compensation [41], since the initially narrow THz pulse will be broadened by the dispersive properties of the fibers. This is a widely researched and well known technical area which will be discussed in Chapter IV with the help of specific experimental tests.

4

THZ-TDS MEASUREMENTS TOWARDS A PLASMA DIAGNOSTIC SYSTEM

4.1 INTRODUCTION

This chapter illustrates the experimental work pursued to understand all the critical aspects of THz-TDS spectroscopy, and devise a detailed strategy to develop a multi functional THz-TDS plasma diagnostic based on optical fibers.

In the first section the different optical set-ups used for the tests are described, and the single components discussed in detail. The common feature is that the linearly polarised THz pulse is generated through photoexcitation of a nonlinear media by a femtosecond infrared laser pulse (GaAs Gallium Arsenide) [8]. TPX lenses, or gold coated off-Axis Parabolic mirrors, focus the radiation on both the sample and the detection elements. The detection of the THz pulse in our experiments is performed with two types of detector, both embodied by a nonlinear photoexcited medium: a InP (Indium Phosphide) photoconductive antenna and a GaP (Gallium phosphide) crystal.

The second section will describe some plasma diagnostics-relevant experimental tests made using commercial THz-TDs spectrometers, with both transmission and reflection set-ups. The objective of these diagnostics is to establish a standard pool of parameters and techniques from which the diagnostic technique can be developed.

The third section will demonstrate the retrieval of useful plasma diagnostic parameters from a table-top plasma source, using a procedure developed by Kolner [42].

The fourth and final section is concerned with the test of the pulse compressor device used to compensate the Group Velocity Delay pulse broadening in optical fibers.

4.2 THZ-TDS SET UP

One of the key strands of this project was to develop and install a THz-TDS spectrometer set up in Frascati. The chosen method employed a coherent Mira Ti:Sapphire mode-locked laser to photoexcite a series of GaAs emitters and Fe++ InP ion implanted detectors. Three optrical configurations with a photoconductive detector were tested in order to demonstrate the feasibility of the system.

For the last one configuration, the emitters and detectors were tested by means of an EO sampling detector, installed to produce a reference signal, chosen for its superior sensitivity and output, using the scheme discussed in 3.1. This allowed to test the emitter functionality and at the same time provide a comparison term for the Photoconductive detector.

MIRA 900 Mode Locked Laser

The Mira laser was characterised for its continuous spectral property, between 400 and 800 nm, as shown in Figure 12

The power range emitted by the Mira measured with a laser power meter during operation ranged between 600 to 1500 mW in continuous-wave (CW) and after mode-locking decreased to 500-1000 mW.

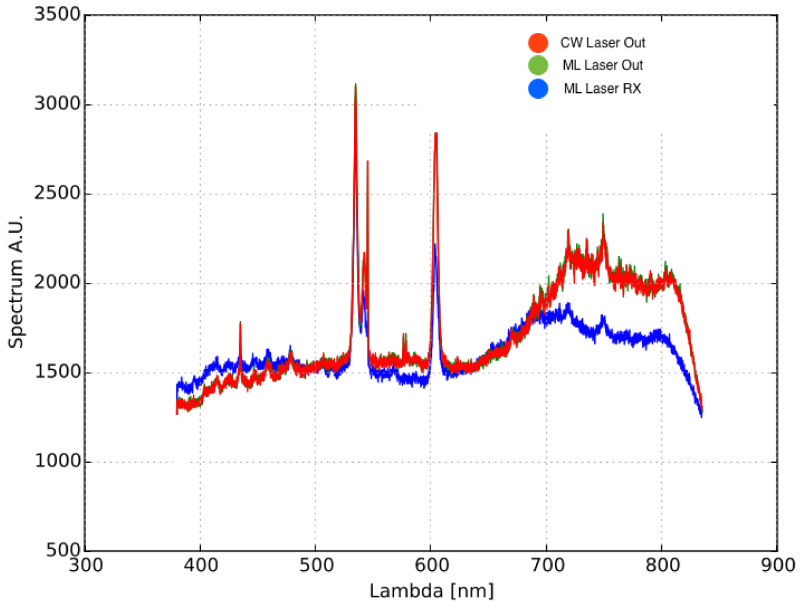

Figure 12: The spectral emission spectrum of the Mira Laser taken at different beam positions (Output of the laser and the receiver position) on the Optical Set-Up. In order to detect the spectral composition a fiber coupled Ocean Optics spectrum analyzer was used.The continuos (Red CW) and mode locked (Green ML) spectra at the output of the laser are coincident, as show in the figure. The spectrum (Blue ML) measured at the receiver position, has the same characteristics of the others beam positions, with lower intensity due to the Beam Splitter progation.

Using a commercial Autocorrelator "Ape-Mini" [43] the time duration of the pulse was checked and calibrated, and ranged from the initial measurement in 2016 of 220 ps to the one in 2018, with a better aligned laser system of 170 ps 1.

Date	τ [ps]
2016	220
2018	170

Table 1: Measured temporal lenght of compressed pulse.

Translation Stage with Stepper Motor

A LTS 300 ThorLabs Translation Stage with Stepper Motor, with minimum translation 2µm, was used to introduce a controlled delay between the pulse pump of the emitter and detector.

Emitter and Detector

The emitter and the detector follow the principle of operation shown in 3.3.2. A FTIR spectrometer Vertex 80V was used to characterise one of the emitters. In order to ascertain the use of the correct semiconductor substrate for the emitter it was checked that the element had the right semiconductor Band Gap. Using the spectrometer an absorption curve was measured using the well know theory described in example in [37]. This operation confirmed that the semiconductor, within the measurement error of the spectrometer, is coherent with the one needed for operation with absorption measured at 1.38 eV and GaAs absorption at 1.43 eV (with 1ev=8.0655 10^3 cm^{-1}). The peculiarity of the photoconductive detector is in its particular configuration as shown in Figure 13 two 15 µm gap in

a perpendicular structure set up, have the capacity of simultaneously detecting the two components of the polarisation as shown in the work of Castro-Camus [40].

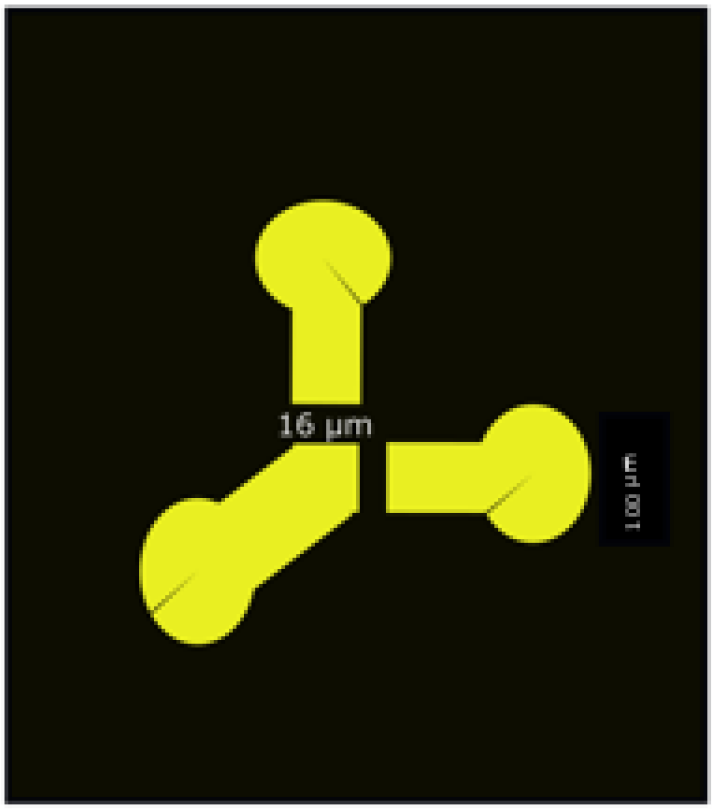

Figure 13: The electric scheme of the photoconductive detector [not to scale]. Three 100 µm gold electrodes are positioned by lithography on a semiconductor substrate in a perpendicular fashion with gap of $\approx$ 16 µ m.

Both photoconductive antennas were mounted onto three axes manual micrometer translation stage. In the electro-optic sampling detector system, the Electro-optical (EO) crystal was mounted onto a rotational stage, in order to find the angle on which is detected the highest signal [44].

4.2.1 *Optical configurations of the set-up*

Three configurations of the experimental set-up were selected and will be illustrated in the following paragraphs.

TPX SET-UP The data presented in the results paragraph (4.2.2) were taken with the typical settings of lock-in amplifier in table 2:

time constant	100ms
Sensitivity	1 nA (photocondutive)/10mV (EO) detection)
filter slope	24 dB-octv
Dynamic reserve	100 dB.

Table 2: Lock-in Settings.

The first configuration as shown in fig. 7 utilised TPX lenses [45] [46] with focal length of 85 mm, commonly used as optical component in tokamaks mm wave diagnostics. The two lenses were arranged one in front of the other, with the emitter and the detector located at the focal length of each lens, following a previous test with the same lens using a commercial THz-TDS spectrometer as shown in [47].

OFF-AXIS PARABOLIC MIRRORS SET-UP In this configuration off-axis parabolic (OAP) mirrors, see fig 14 were introduced to improve the focus of the THz beam onto the detector, and to remove TPX spectral absorption. In the first approach, the photoconductive detector was illuminated by the IR pulse on one side with the electrode, and by the THz beam on the other.

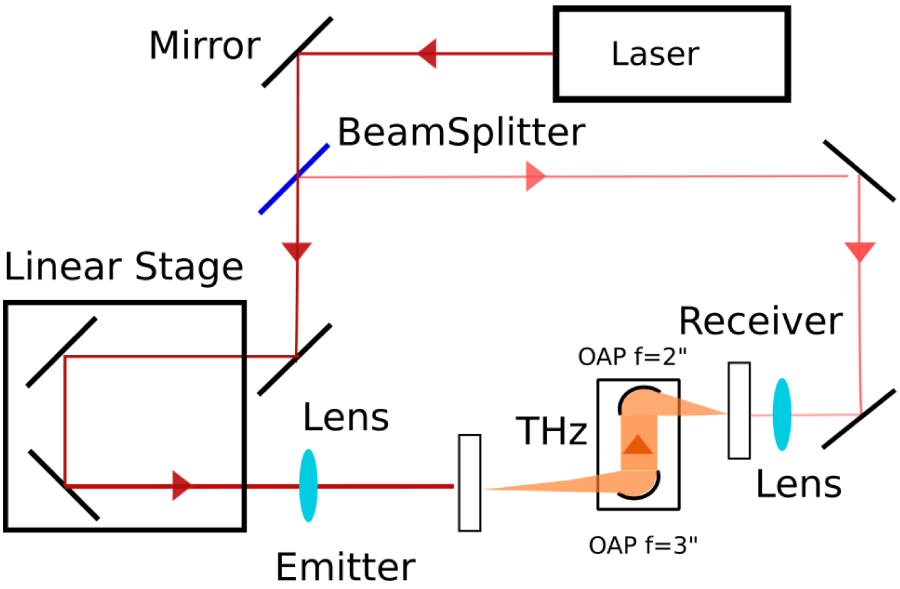

Figure 14: In the first configuration off axis paraboloids f_1=3", and f_2=2" used to focussed the THz beam on the detector. The probe laser beam shine on the opposing face of the photoconductive antenna in respect to the THz beam.

PHOTOCONDUCTIVE ALIGNMENT The alignment procedure comprises of two essential phases: general alignment, and fine tuning.

The general alignment of the laser system with beam splitter and mirrors is a crucial preliminary step, necessary in order to achieve stable propagation on the linear mechanical stage. An error at this stage could lead to an inaccurate scanning of the pulse, lacking a stable and reproducible illumination of the emitter. The second phase of the alignment was done using the following procedure, centred around the OAP system.

1. A beam diffuser made of bond paper was placed in the same position as the THz emitter, generating a spherical wavefront of IR light which followed the same path of the THz.

2. It was observed that the after propagation through the OAP system, the alignment between the focus light of the diffused beam was collinear to the IR detector gate beam.

3. Blocking the emission branch beam, the detector element was arranged in the path of the detection branch.

4. The resistance of one of the gaps of the photoconductive antenna detector was minimised to a value of 35 kΩ with 400 mW of average laser power

5. The diffuser was replaced by the photoconductive antenna and aligned on the freed emission path reducing the resistance of the emitter to a typical value of 40 kΩ .

In the second approach, see fig 15, the detector was illuminated by the IR laser beam trough an hole inside the OAP and it shined colinearly to the THz beam on the detector, whether was a photoconductive detector or EO sampling crystal.

ELECTRO-OPTICAL ALIGNMENT In order to test the emitter capabilities and obtain a reference spectrum, a new detector was put in place: an EO sampling system based on GaP <110> crystal, more sensitive and with higher output signal and a frequency response up to 1.5 THz.

The elements of the EO detector alignment followed the arrangement indicated in Figure 9 , comprising of a GaP crystal, a quarter-wave plate, a Wollaston prism and two balanced photodiodes. This ensemble constituted the detector configuration shown in Fig 15.

Following the operation procedure explained in section 3.3.4.2 the system was successfully aligned as by the following method:

1. Alignment of the system without the GaP present, to ensure both photodiodes received the signal.

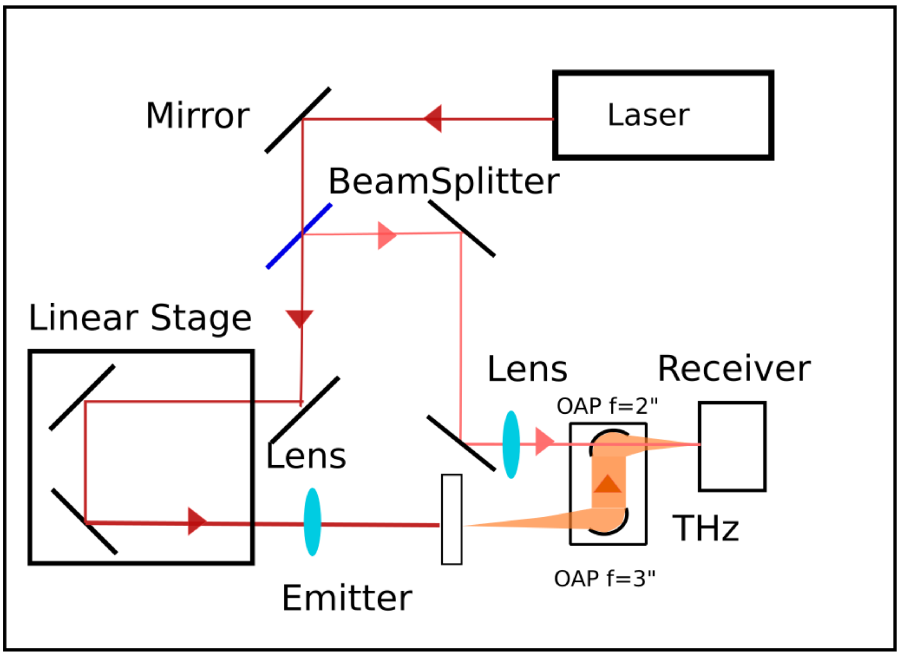

Figure 15: In the second configuration off axis paraboloids f_1=3", and f_2=2" used to focalize the THz beam on the detector. The probe laser beam shine trough the hole in the perforated 2" OAP and hit the EO crystal collineary to the THz beam.

2. Rotation of the quarter-wave plate until there was no signal seen from the balanced photodiodes.

3. The previous step was repeated with the GaP inserted, to obtain zero output signal

4.2.2 *Results and Conclusions*

Different configurations were tested in order to verify the functioning capacity of photoconductive emitter and polarizer antenna pair. To analyse the properties of the emitter, an EO sampling device was installed. Comparisons between the electric field detected by the photoconductive antenna electrodes (depicted in Figure 16) and the one produced by the EO detector in Figure 18 demonstrated that the photoconductive antenna possesses a low THz bandwidth response, lacking the tempo-

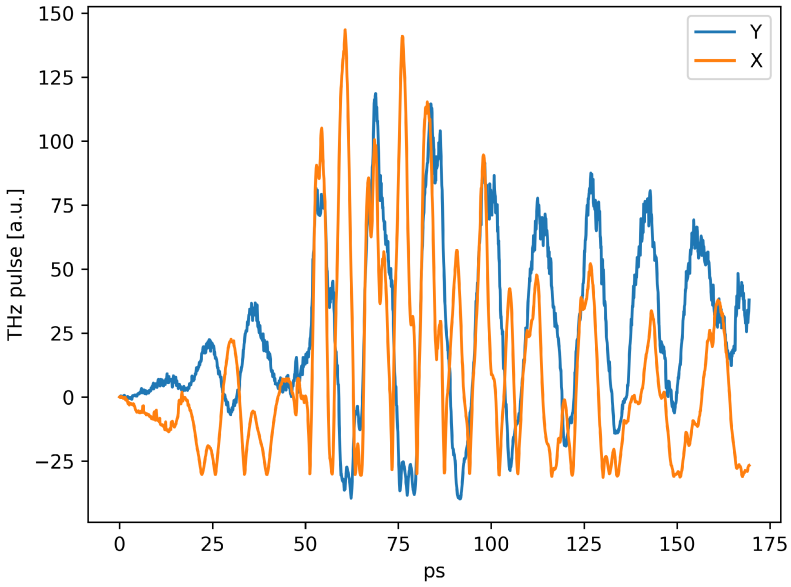

Figure 16: THz pulse measured with the X and Y polarisation electrodes of the photoconductive antenna in Frascati.

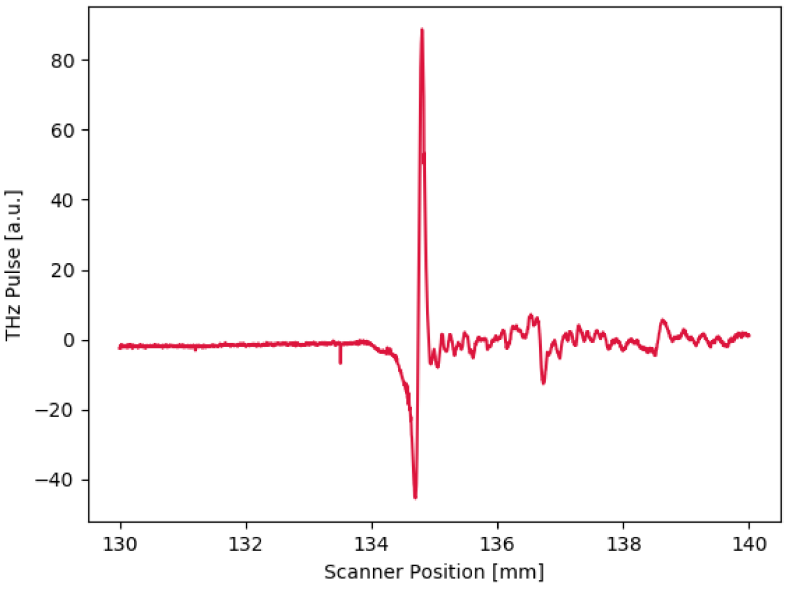

Figure 17: THz pulse obtained with the Electro Optical sampling system in Frascati.

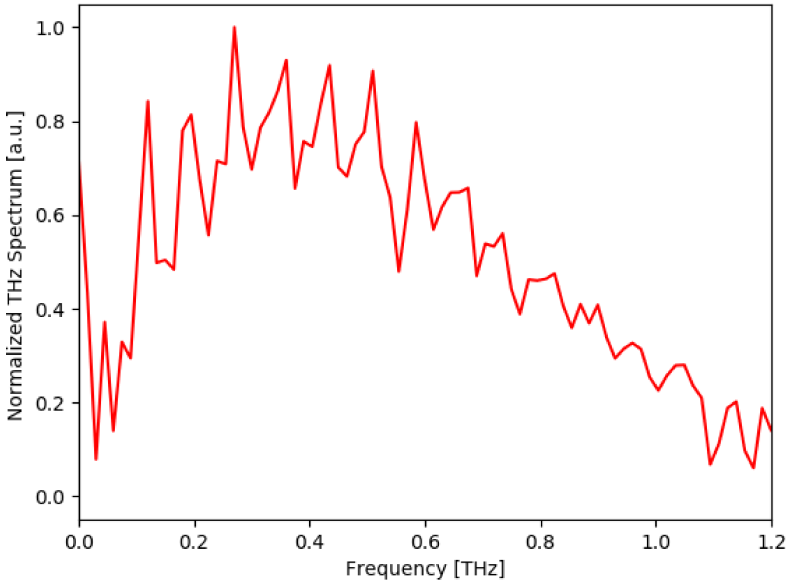

Figure 18: Normalized spectrum of the THz Electro Optical sampling pulse of Fig. 17. The oscillating artifacts in the spectrum are due to the presence of reflection spikes in the pulse in Fig. 17, they will be removed with thorough alignment and arrangement of the setup.

ral resolution to detect the THz pulse cycle variation, and this is showed by comparing the time scales of the pulse in the photoconductive case and in the EO crystal case, which is, in the photoconductive detector measurement ten times the required values.

4.3 PLASMA DIAGNOSTICS-RELEVANT EXPERIMENTAL TESTS

A number of tests were devised and performed to explore the potential of the THz technique regarding its use as Plasma Diagnostic. By studying the optical transmission in the THz range of different samples in various experimental conditions, the potential and the requirements of THz-TDS spectrometers and of the analysis software was explored and tested in depth. The transmission of a birefringent element was measured using the same setup. Using a reflectometry set-up, studies of the technique potential were made employing both simple and complex geometry samples. All the tests were performed using the equipment of CIO (Centro de Investigaciones en Optica) of Leon (Mexico).

4.4 VALIDATION OF TRASMISSION MEASUREMENTS

What follows is the description of the test devised to extract the index of refraction $\tilde{n}$ from a sample of known thickness. This is an application of the standard experimental procedure of THz-TDS spectroscopy, where a complete analysis of the data is performed, and common issues are located, such the zero padding of the signal [48]. In the last section of the chapter these same procedures will be applied to plasma measurements, and have to be considered for future reference in a practical tokamak diagnostics scenario that will use a similar principle of operation.

4.4.1 *Preparation of the Sample*

The sample preparation in the transmission measurement was realised by a Prusa i3 commercial 3D printer with a 0.4 mm nozzle for 1.75 mm filament and layer height from 0.05 mm. The filament used were PLA (Polylactic acid) and Bendlay. The sample manufactured was a disk of 1 inch diameter (2.54 cm) and of various transverse size: 1,3,7 and 10 mm.

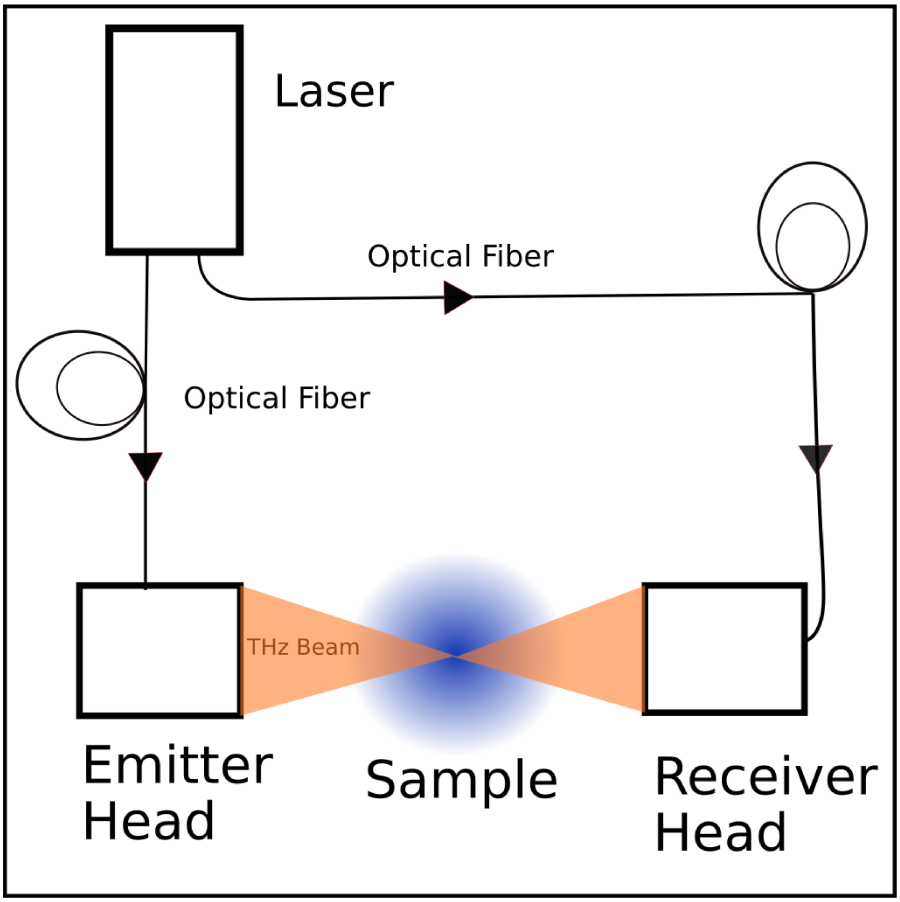

Figure 19: Experimental set up Picometrix T-Gauge 5000 at CIO showing emission and detection heads pumped by a 1064 nm fs laser with 100 MHz of rate. The laser pulse of 80 fs is transmitted trough proprietary polarising mantaining fiber optics. The sample is put in between the two Heads.

The objective of the measurement is to estimate the index of refraction and the absorption index of a sample of known thickness using THz-TDS.

4.4.2 *Description of the experimental apparatus*

The measurement was done with a commercial spectrometer Picometrix T-Gauge 5000. The optical system featured a sample holder, a transmission and a detection head as shown in Figure 19. This was mounted onto an optical rail. The two heads, equipped with a system of lens with effective focal length of 6.5 cm, were pumped by a 100 fs laser pulse with central wavelength of 1100 nm, through two 5 meter optical fibers. The nominal bandwidth of the system was of 0.2-3 THz but the experimental bandwidth actually used for the test was 0.2-1.6 THz, since the spectral power signal over 1.6 THz is 10 dB lower than the maximum signal detected. The sample was a disk 1 mm thick, 1 inch wide, 3D printed with Polylactic acid (PLA).

THEORY OF THE MEASUREMENT The time domain propagations of the THz pulse (E_{smp} (t)) are recorded and compared with and without the sample. Performing a Fourier trasform enables the derivation of the transmission spectra of the two pulses $S_{ref}(\omega)$ and $S_{smp}(\omega)$, and consequently the phase difference $\Delta\varphi = \varphi_{smp} - \varphi_{ref}$ between the two. With the assumption of an optically thick sample ($d >> \lambda$), using equation 38 it is possible to derive the index of refraction and the absorption index as a function of the frequency [49].

$$n(\omega) = 1 - \frac{c}{d\omega}\Delta\phi \tag{38}$$

$$k(\omega) = -\frac{c}{d\omega}\ln\left(\frac{E(\omega)_{smp}}{E(\omega)_{ref}}\right) \tag{39}$$

Where c is the speed of light , and d is the thickness of the sample.

DATA ANALYSIS The data analysis was performed using bespoke coded software in Python. The data acquired by the spectrometer was preprocessed as follows:

- Subtraction of the field zero value to the data, through removal of the DC noise present.
- Apodisation of the signal by using a windowing function, in this experiment a Savitzky-Golay filter [50] centered on the peak for the THz pulse, resulting in removal of the high frequency noise and the double reflections of the pulse.

The Fourier spectra were retrieved by fast Fourier transform, from which the transmission function $H(\omega) = \frac{S_{ref}(\omega)}{S_{smp}(\omega)}$, shown in fig. 21, was calculated. The phase difference between the two pulses is obtained as the argument of H and then unwrapped in order to add and subtract a 2π factor.

The index of refraction and the absorption index were calculated using eq. 38.

RESULTS Following the data analysis procedure, the following observations were made:

- The data presented oscillations, compatible with a Fabry-Perot effect, originating from the thickness of the sample.
- Beyond 0.6 THz there is a large increase in the nise, due to the spectral characteristics of the sample.
- Water vapour lines were detected in the spectrum, expected ias measurement conducted in air.

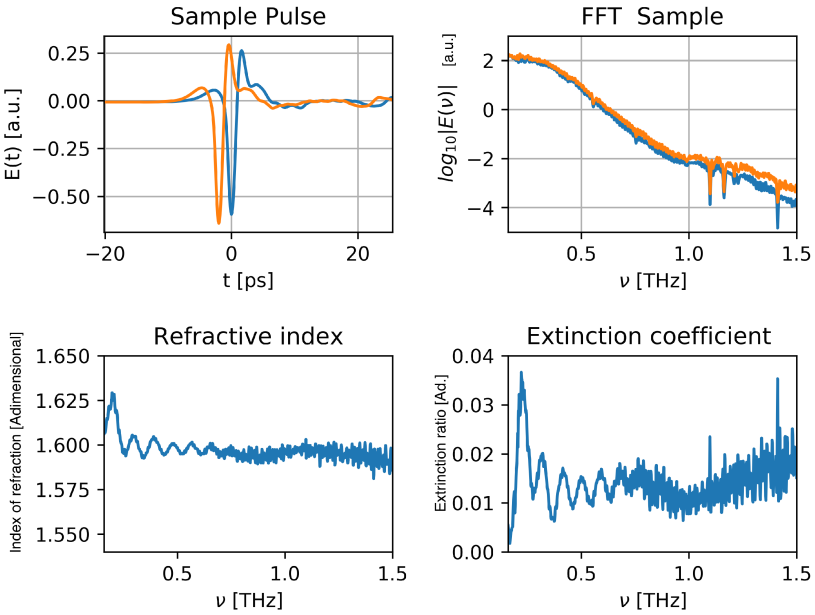

Figure 20: top left: PLA disk THz pulse, top right: Spectrum, bottom left: Index of refraction, bottom right: extinction index. In orange the pulse and FFT of the reference spectrum, in blue the ones of the disk sample and the frequency is indicated with ν.

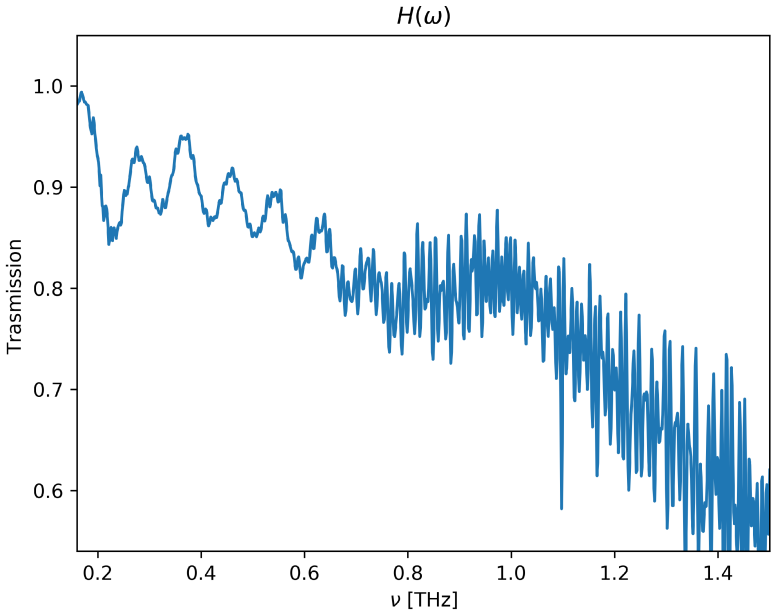

Figure 21: The function H(ω) (see text for description)

- Beyond 1.6 THz (not showed), the noise was predominant.

The refraction index was estimated (see Figure 20) in accordance with the literature value for PLA, between 1.5 and 1.8 [51].

More complex algorithms [49], that utilize minimization function to derive the index of refraction with more accuracy, can be utilised to remove the Fabry-Perot effect, but for the scope of the test were not considered useful.

The water vapor lines can be mitigated by employing a vacuum set-up or a nitrogen flux.

4.5 VALIDATION OF POLARIMETRY MEASUREMENTS

The following section demonstrates how to study the transmission properties of a birefringent element using THz-TDS.

Experimental Set up

By using the same optical set-up of the PLA index of refraction measurement, a 3D printed carved disk was positioned onto a rotating holder in the sample position, with the zero position indicated by the grooves of the disk placed parallel to horizontal polarisation of the THz wave.

Theory of experimentation

The carved disk (Figure 22) was fabricated using a 3D printer using the construction theory for a birefringent element shown in [52], the optical element was created by stacking alternate slabs of two media carrying two different refractive indices, n_1

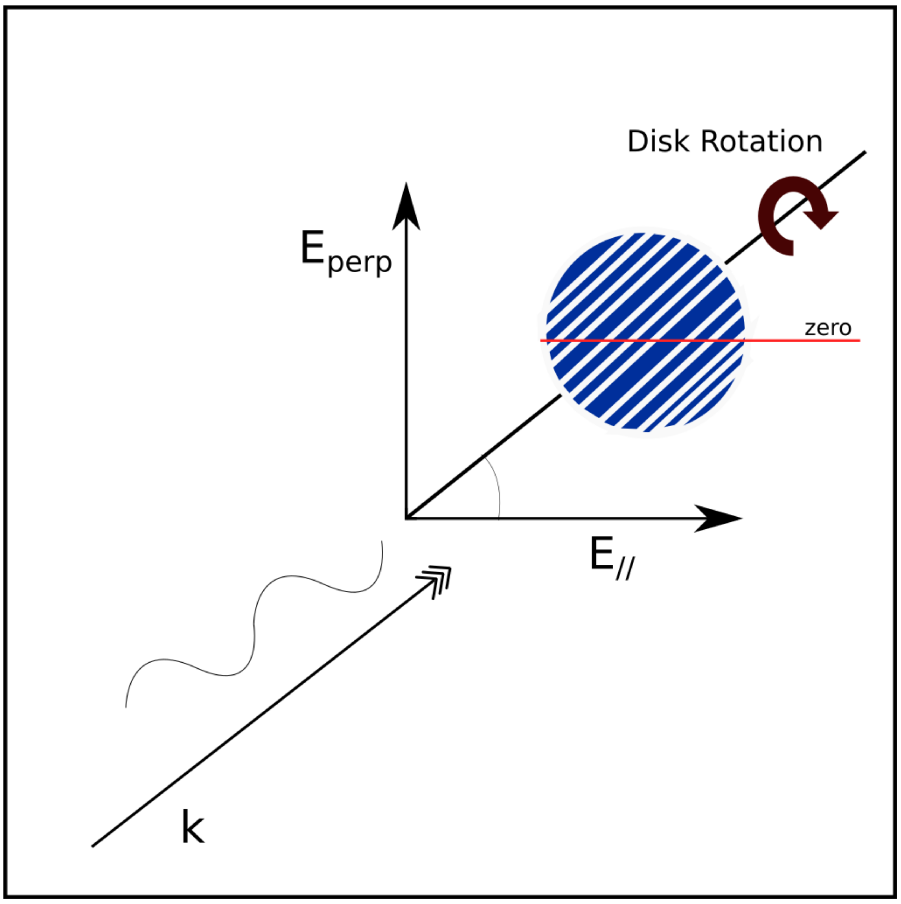

Figure 22: The position of the carved disk in respect to the incident (horizontally polarised) THz electric field. E_{perp} is the perpendicular electric field component, $E_{//}$ the parallel component, k the propagation vector. The reference zero angular position for the disk is defined as when the grooves are parallel to the $E_{//}$ polarisation vector.

and n_2, of respective thicknesses L_1 and L_2, forming a disk as shown in the figure 22. However, this model is valid in practice only if the dimensions of the slabs slightly exceed the THz wavelengths. For higher frequencies, scattering and waveguiding effects will occur , limiting the frequency window of operation for the device. Interaction of a composite material system and a THz wave, modelled by a quasi-static effective medium theory (EMT) can be utilised if the wavelength exceeds the dimension of the individual components. . The resulting optical properties of this system can be described in the case of a quasi-static regime analogously to a plate capacitance. The quasi-static refractive indices $n_{TE,0}$ and $n_{TM,0}$ for a polarisation of the electrical field parallel and perpendicular to the layer, respectively, are given by:

$$n_{TE,0}^2 = f_1 n_1^2 + f_2 n_2^2 \tag{40}$$

$$n_{TM,0}^2 = (\frac{f_1}{n_1^2} + \frac{f_2}{n_2^2})^{-1} \tag{41}$$

where f_1 and f_2 are the volumetric fractions of the individual components. This quasi-static model is violated when the period of the structure, $\Lambda = L1 + L2$, approaches the magnitude of the THz wavelength. A second order EMT can be derived as shown in [52] as a function of Λ and the wavelength of the incident electromagnetic wave λ:

$$n_{TE}^2 = n_{TE,0}^2 + \frac{1}{3}(\frac{\Lambda}{\lambda}\pi f_1 f_2 (n_1^2 - n_2^2))^2 \tag{42}$$

$$n_{TM}^2 = n_{TM,0}^2 + \frac{1}{3}(\frac{\Lambda}{\lambda}\pi f_1 f_2 (\frac{1}{n_1^2} - \frac{1}{n_2^2}) n_{TE,0} n_{TM,0}^3)^2 \tag{43}$$

The parameters chosen in the test lead to to $n_{TE,0} = 1.27$ and $n_{TM,0} = 1.17$, for index $n_1 = n_{air} = 1$ and $n_2 = n_{Bendlay} = 1.5$, and the chosen values for Λ=800μm and $f_1 = f_2 = 0.5$.

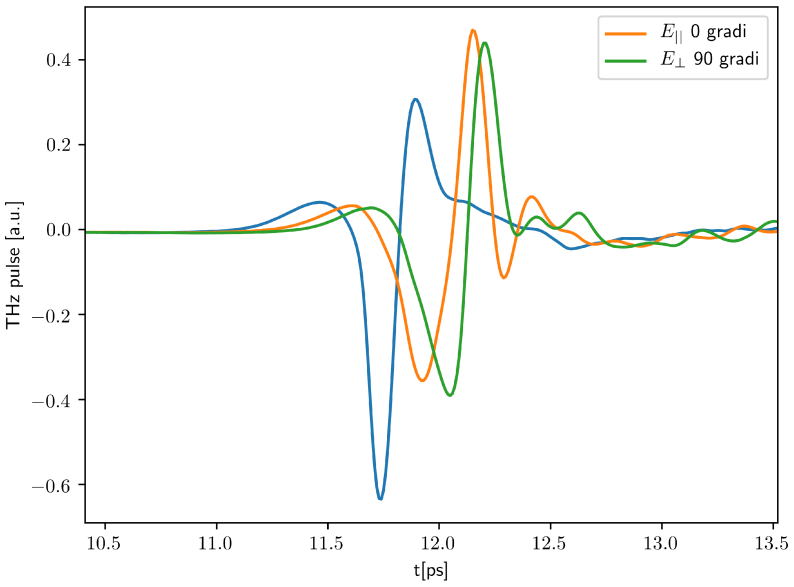

Figure 23: THz Pulses of the birefringence experiment, in blue the reference signal, in orange the pulse $E_{||}$ with the disk at zero degree and in green with the disk at $E_{\perp}$ ninety degree with respect to the plane of polarisation of the THz pulse.

CONCLUSIONS Birefringence is the variation of the index of refraction between the two optical axes, corresponding to a variation in the propagating time of the pulses inside the element. This phenomenon can be characterised by observing four key variations between the pulses, namely: propagation time of the peak (Fig 23), shape of the pulse, Fourier spectrum (Fig. 24) and index of refraction (Fig. 25).

The effect at higher frequencies where the index of refraction is $n = 1.3$) to both the directions of propagation is not expected (it is supposed to be different between the two order of propagation).

The effects of the birefringence are visible in the refraction index up to 500 GHz, at higher frequencies producing effects which are not expected by the method of production. To limit absorption, but ensure visible birefringence effects, the thick-

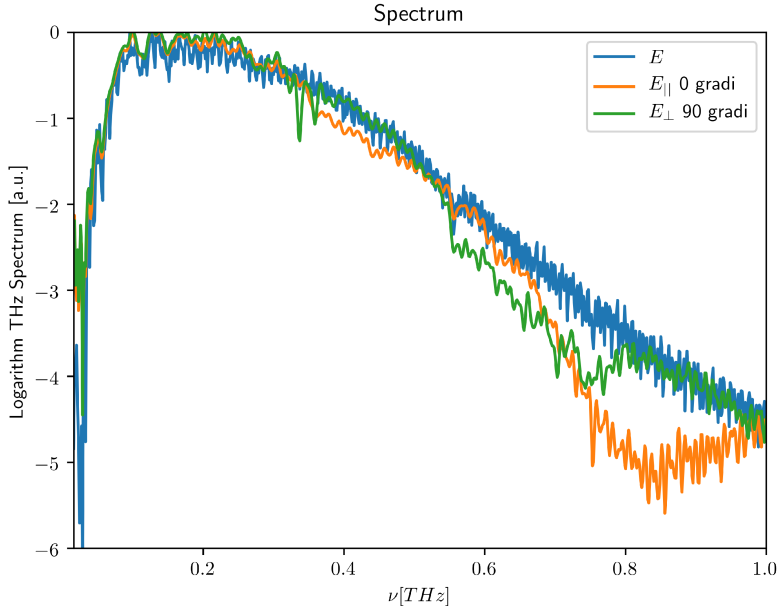

Figure 24: Spectra of the birefringence experiment: in blue the reference signal, in orange the pulse $E_{||}$ with the disk at zero degree and in green with the disk at $E_{\perp}$ ninety degree with respect to the plane of polarisation of the THz pulse.

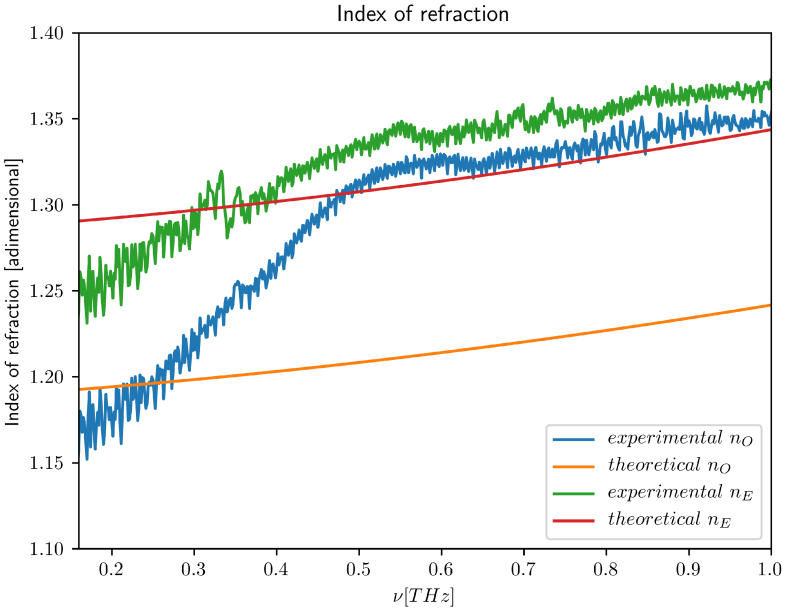

Figure 25: Index of refraction of the birefringence sample, in blue and green respectively the n_{TE} and n_{TM} experimental index, in red and orange the theoretical ones.

ness of the disk was chosen at 3mm. When the wavelength of the radiation is greater than the geometrical dimension of the graves, the sample is seen by the wave as a whole and so the birefringent effect disappears and so in both direction the index of refraction arrive to n=1.3.

4.6 VALIDATION OF REFLECTOMETRY MEASUREMENTS

In the THz reflectometry configuration, sheets of paper with a range of thickness were measured and an electronic device presenting a complex geometry (Kindle [registered mark]) was mapped in the x, y plane to demonstrate the resolution capability of reflectometry in the time domain.

DESCRIPTION OF THE EXPERIMENTAL APPARATUS The reflectometry measurement was performed with a commercial spectrometer a Picometrix T-gauge 500. The optical system was composed by a transmission head, a detection head, a collinear adapter with a focusing length of 3 inches as shown in Figure 26, all mounted onto a motorised platform that can scan a plane (X,Y) and move in the Z direction, and a sample holder.

The two heads were mounted onto the collinear adapter, and pumped by a 100 fs laser pulse with central wavelength of 1100 nm, through two 5 metre optical fibres and the sample holder was positioned under the collinear adapter. A slab of reflecting metal was positioned congruent to the sample holder, where the optimal focal distance was found by maximising the signal.

Up to six planes of paper were positioned onto the holder, and each time measured. The same approach was taken in measuring the electronic device: a slab of reflecting metal placed in the same position and height of the device, in order to find the optimal reference signal. The scan was made by fixing the opti-

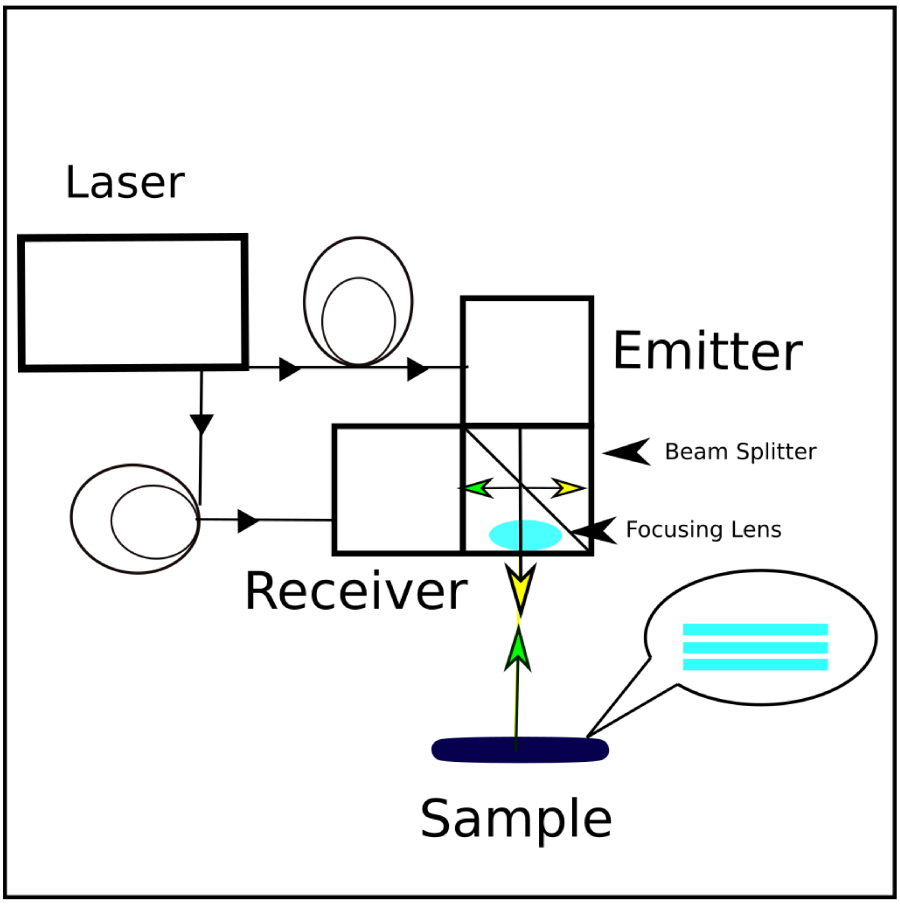

Figure 26: Experimental set up. An emission head and a Detection head pumped by a fs laser in reflectometry mode, with a B/S as facing part element, after that the beam is focused by a lens of focal length of 3 inches. The stacked paper sheets are shown in the scheme as sample, expanded in the balloon for visual clarity.

cal stage on the Y axis position and scanning in the x-direction measuring for each step a THz pulse as show in fig. 31 at each point a THz pulse of the system was recorded.

Data Analysis

In the case of the electronic device only a qualitative study was possible as the material thicknesses and transmission properties at different points are calculable from the different return times of the THz pulse reflection peaks. Consequently, a study of the reflection properties done on each element spectrum (0.1 to 1.6 THz) was the basis of the construction of a X-Y contrast map displaying the most visible frequency reflections.

To improve our understanding of the reflection technique a simpler media was observed: a stack of paper sheets as shown in Fig. 26. For the thinnest paper sample, no double reflection nor detectable variation of the optical path length should be expected, given that the index of refraction of paper n_{paper} varies along 1.2 and 1.5 in the THz range. The distance from each sheet of paper can be estimated by taking into account that in free air, radiation will propagate for 0.3 mm in 1 ps.

RESULTS A study of the imaging of paper planes was done, providing a less complex framework beneficial for studying the different propagation properties of the pulse. The number of planes corresponds to the number of the peaks in the reflected pulse. The travelling time of the pulse corresponds to the distance of each paper, in the case of the experiment done with three planes (see Figure 27), measuring the distance bewteen each peaks is possible to deduce that the separation of the planes are 0.7 mm for the first two and 1.3 for the second. In the reflected spectrum frequencies, the number of the holes seems

to be connected to the planes of paper see figure 28 as the frequencies shifting, but the exact reason and a law to describe it has to be still found.

For reference are shown the other study made with different number of paper sheet (from one to seven) and their respectively pulse and spectra in fig. 29 and fig. 30.

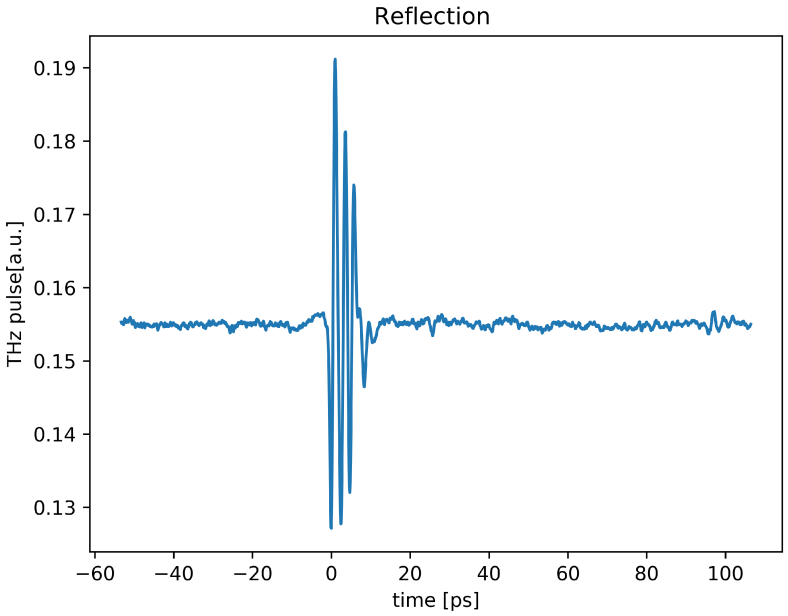

Figure 27: Reflected THz pulse of a sample made of three stacked sheets of paper.

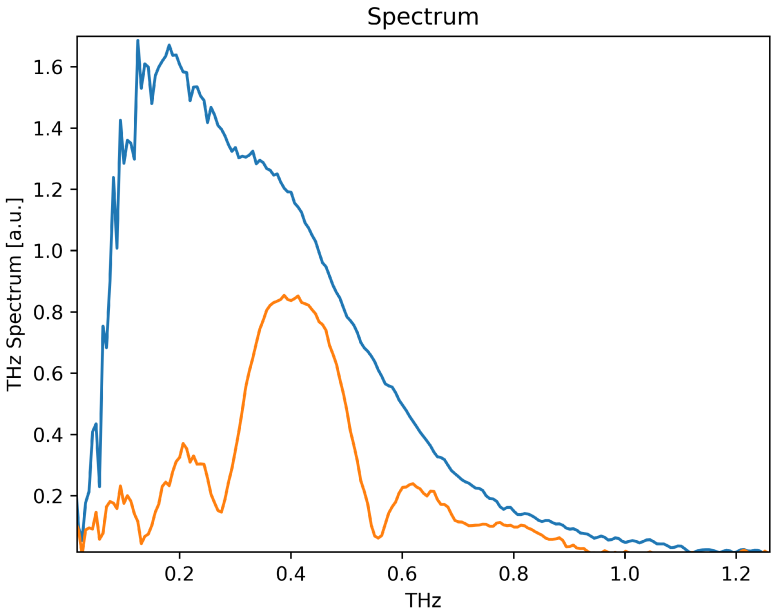

Figure 28: Spectrum of the reference pulse (blue) and reflected pulse from the stacked paper sheets samples (orange).

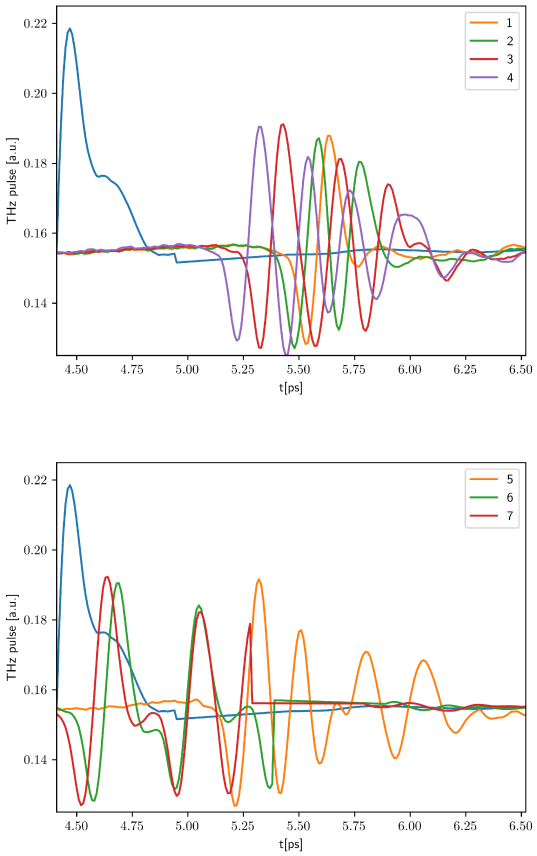

Figure 29: Time domain pulse reflection with stackes of paper, with in blue the metal background reference reflection. In the legend are indicated the numbers of paper put in the stack.

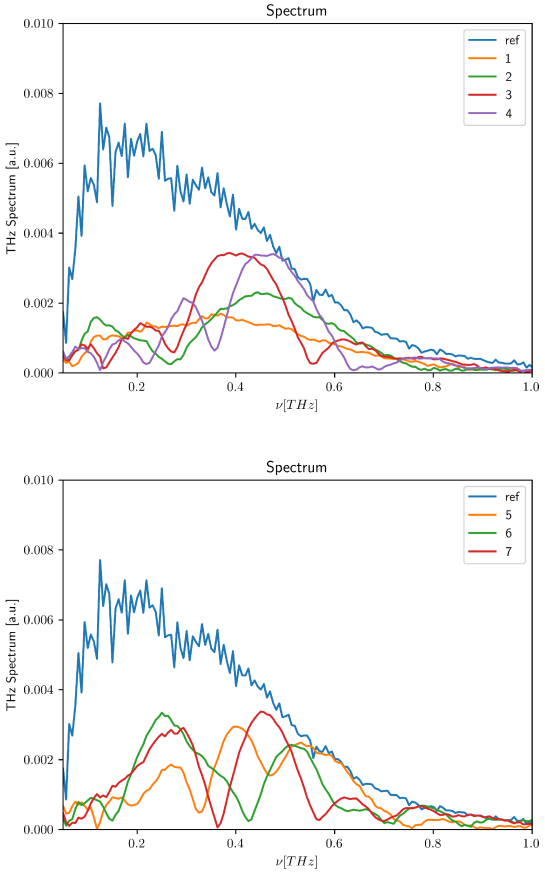

Figure 30: Spectra of the THz reflection with stacked of paper sheet, with in blue the metal background reference reflection. In the top image are represented the spectra from 1 to 4 stacked papers; in the bottom image are represented the spectra from 5 to 7 stacked papers. The difference in intensity between Spectra can be explained by differences in the alignment of the sheets of paper in the stack. In the legend the number of paper in the stack is indicated.

In the case of the X-Y scan output of the electronic device, it can be analysed in two different ways. This is a guideline of how to diagnose a given plasma region. For every point of the scanned map the recorded THz pulse, shown in Figure 32, individuated by the various reflected electric field peak is reconnected to its thickness and index of refraction of the device internal components. The other technique is to map the reflected spectrum for each X-Y point and studying the spectral properties of the reflection as shown in the Kindle [registered mark] experiment. This method enables a descriptive map of the device with the maximum contrast image as show in fig. 32. In fig. 33 and fig. 34 are shown the pulses and respective spectra of fixed X and Y step to present a time and frequency slice of the measured points.

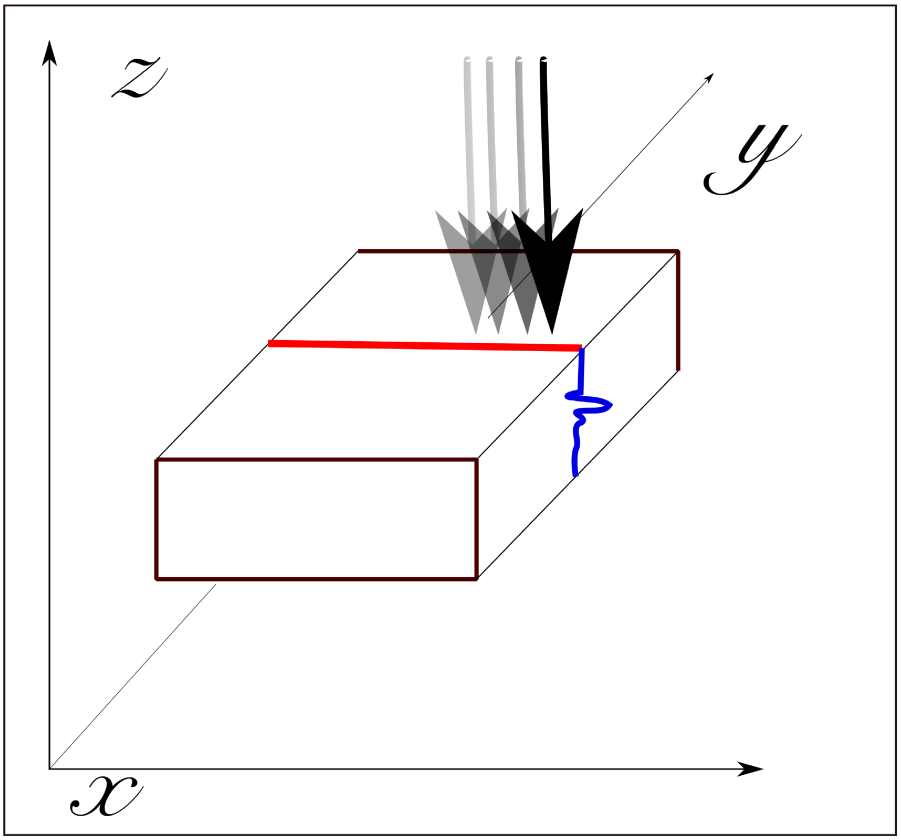

Figure 31: Reference axes for the reflectometry scan of the Kindle, here represented by the rectangular box. Fixing y coordinate, a scan along the x axis was done. (Xsteps=358,Ysteps=240, 0.5 mm for each step). In red is represented the scanning path for a fixed y, with the THz beam direction indicated by the vertical arrows. In blue is represented the THz pulse propagating inside the sample before reflection.

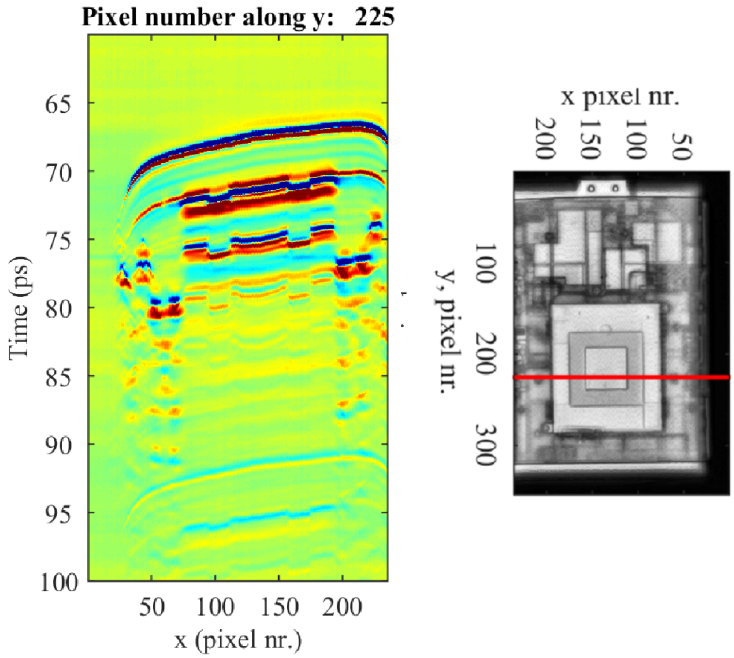

Figure 32: (left) The B scan of the Kindle (registered mark). Axes defined in Fig. 27: a scan along the x direction, with fixing Y, showing the THz pulse reflection (Z axis in ps) of the internal part of the electronic device. (rigth) An XY scan of the electronic device, showing the contrast figure of the maximum peak reflections from all the frequencies received.

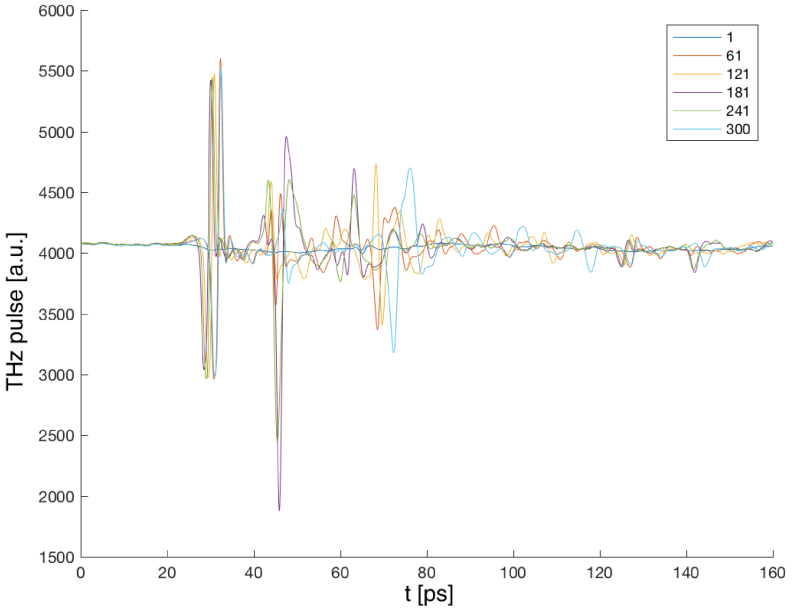

Figure 33: To better show the pulses acquired during experimentation, fixing X step =140, THz pulses where taken at different Y step positions. As shown in legend by different map colour the steps are: Ysteps=1, 61,121,181,241,300.

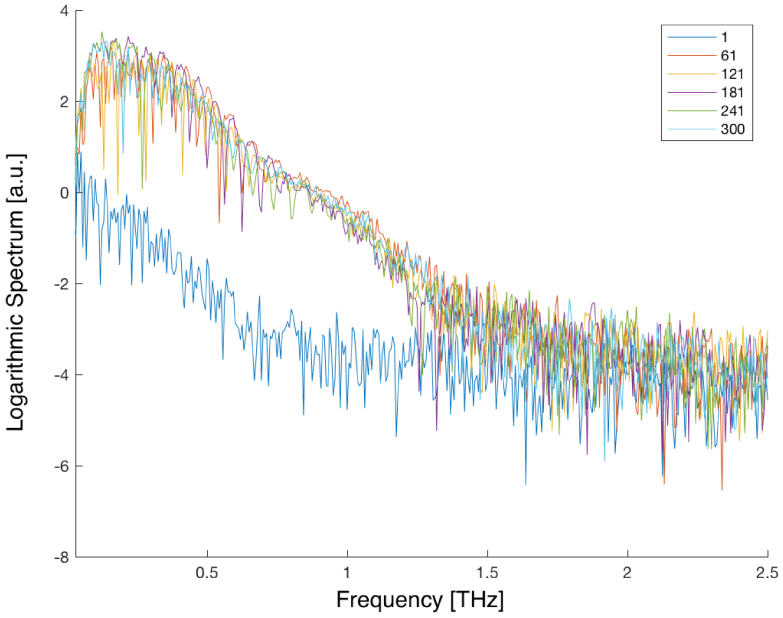

Figure 34: Using the pulses shown in 33 are shown different Spectrum calculated by fast Fourier transforms in logarithmic scale. In the same way was taken at the X step =140 and then changed the Y step. As shown in legend by different map colour the steps are: Ysteps=1,61,121,181,241,300.

4.7 EXAMPLE OF PLASMA MEASUREMENTS

Gas	Symbol	Type	Current [A]	Power [W]
Mercury	Hg	HPK125	n-a	n-a
Mercury	Hg	93136E	0.9	90
Cesium	Cs	93105E	0.9	10
Zinc	Zn	93145	0.9	25
Sodium	Na	93122E	1	2

Table 3: Characteristics of Philips spectroscopic lamps.

The use of THz-TDS for plasmas characterisation has been greatly developed following the pioneering study of Jamison [53] in 2003 and Kolner [42] in 2008. Kang et al. [54] in 2017 added interesting results specific to plasma diagnostics. Under the assumption of a homogeneous plasma slab, electron density and collision rates can be obtained from the spectral data. To improve the understanding of the interaction between THz radiation and plasma sources, and to obtain a preliminary test of the effective diagnostic potential, the THz-TDS transmission was studied [55] in plasma present in standard spectroscopic lamps [56] containing different chemical species, with the characteristic a shown in table 3. These devices produce a high-density plasma (up to 10^{20} m^{-3}) as a result of arc discharge inside the gas that ionize the gas atoms present in the bulb and generate a steady plasma source. They are widely used in spectroscopy as sources of reference spectral lines, or as broadband sources useful for the calibration of spectrometers (for example in electron cyclotron emission diagnostics) in the region where plasma properties approach a blackbody.

EXPERIMENTAL SET-UP A THz generation and detection was provided by a Ti:Sapphire regenerative amplifier laser, with

pulse duration of 35 fs, 5 kHz repetition rate, and centre wavelength 800 nm. The laser pulse is split into two beams:

1. A pump beam, generating the THz probe through spintronic effects [57], producing a THz beam of width less than 1 mm at the lamp
2. A gate beam for EO sampling of the THz electric field amplitude, via a 200 µm <110> GaP crystal [58]

By scanning the path difference between emitter and receiver sections, the electric field versus time, i.e. the THz waveform, was obtained. The corresponding spectrum was calculated via standard Fourier Transform.

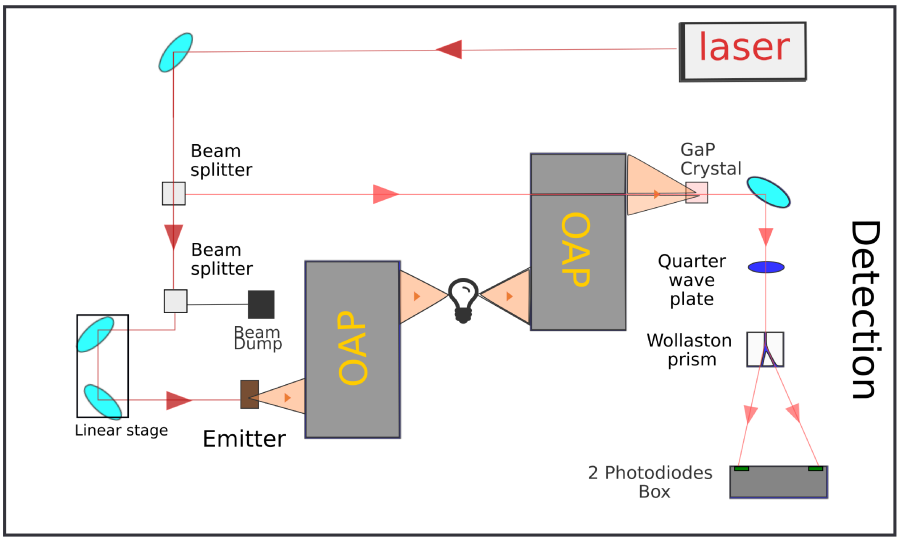

Figure 35: THz-TDS experimental set up for spectroscopic lamps plasma measurements. The lamp is placed in the focal point of a matching pair of off- Axis Paraboloids (OAP) so that the THz beam crosses the plasma in the region of maximum density.

MEASUREMENTS Two types of spectroscopic lamps were used as plasma source: HPK125 (Hg) single quartz bulb and a 931(xx) series lamp with double glass bulbs. Both lamps operate at 1A current between 200 V and 400 V. The THz-TDS

system used for the measurements is shown in Figure 35. The optical properties of the lamp bulbs strongly limit the spectral transmission bandwidth. HPK125, with its 1 mm thick single quartz bulb, provided the broader spectral frequency range. In absence of a heat sink element, the measurement time was regrettably limited to a few minutes by the overheating of the THz setup. The Philips 931xx series has a second external glass bulb designed to improve the vacuum seal. This is very effective for thermal insulation, hence permitting a longer measurement time, but dramatically reduces the amplitude of the trasmitted THz pulse (fig. 36) and the width of THz transmission spectra as shown in the experimental transmission spectra of both lamp types in Figure 38.

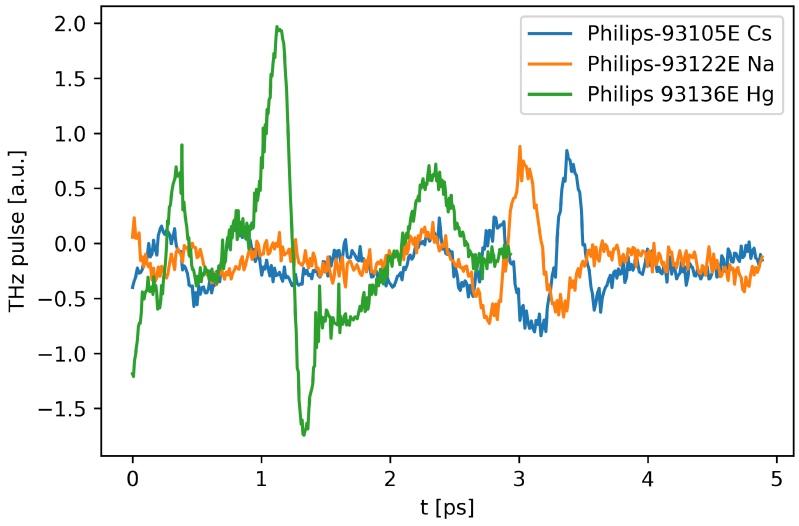

Figure 36: THz Pulses from Cs, Hg (9136E) , and Na lamps measured in identical experimental conditions. The Hg (HPK) pulse is not showed because the scale of the pulses intensity were not comparable.

The transmission property of the quartz and glass bulbs was observed to significantly change with temperature, due to both thermal expansion and refraction index variation. To compensate for this effect we measured a reference spectra immediately

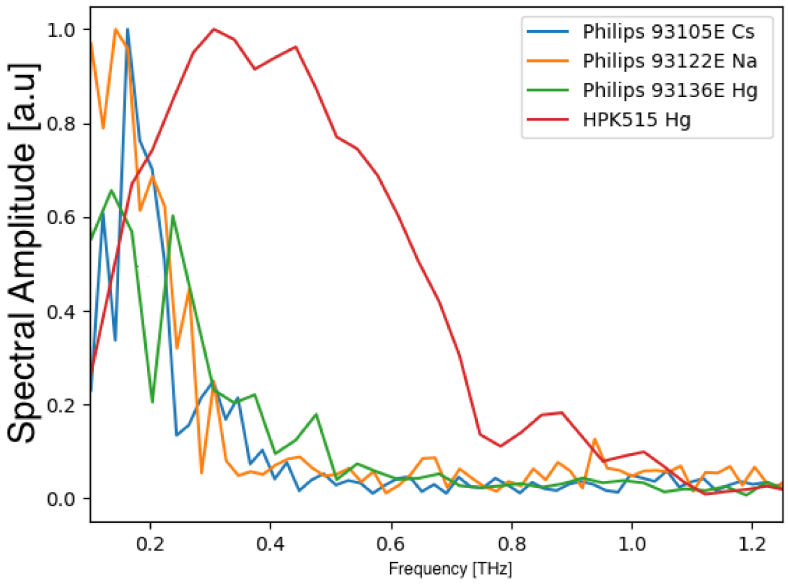

Figure 37: Normalized transmission spectra from Cs, Hg, and Na lamps measured in identical experimental conditions. The plasma frequency lies in the lower part of the spectrum (<100 GHz). The lower bandwidth of the 931xx lamps, with a 0.5 THz upper limit, double bulb arrangement, in which the absoption is increased by the two layers of glass.

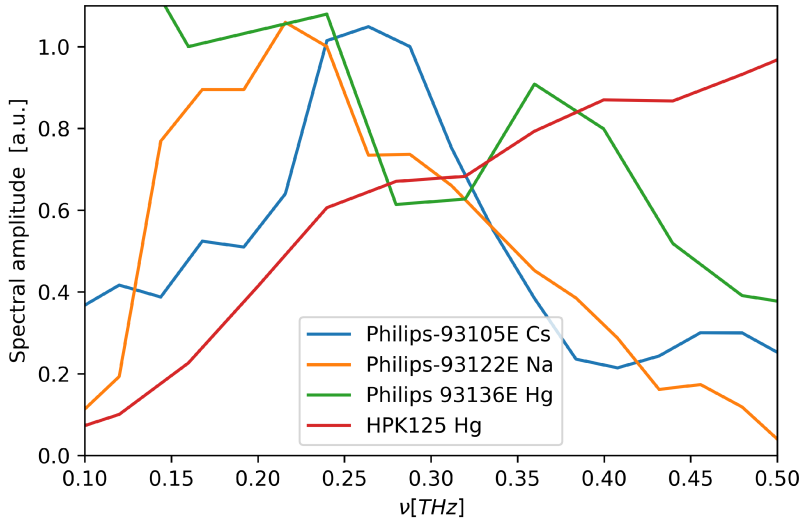

Figure 38: Zoom of Fig. 38 of the trasmitted spectra from Cs, Hg, and Na lamps measured in identical experimental conditions under 0.5 THz.

after switching the lamps off, thus removing the plasma discharge. This technique can be refined in future measurements by alternating plasma and reference measurements with a modulation of the lamp power supply synchronised with the data acquisition. The measured spectral bandwidth is approximately 0.1-1.1 THz for HPK125 and 0.1- 0.5 THz for Philips 931xx.

DATA ANALYSIS With the aim of providing a demonstration of the system diagnostic potential, an estimate of the plasma density was obtained by comparing the plasma spectra S_{smp} with the reference S_{ref}, in the frequency domain, making basic assumptions of the unknown experimental parameters. The transmission function of the plasma is the ratio between plasma and reference spectra, as in Figure 38

By using the model proposed by Kolner et al. [3] for a plasma slab of uniform density in the cold plasma approximation, H is written (in the frequency domain) as:

$$H(\omega, n_e, \nu_e) = \frac{S_{smp}(\omega)}{S_{ref}(\omega)} = exp(i\frac{\omega L}{c}(1 - n(\omega, n_e, \nu_e))) \quad (44)$$

where n_e is the electron plasma density, ν_e the electron collision frequency, $n(\omega, n_e, \nu_e)$, the complex index of refraction, ω the pulsation (radian-frequency) of the THz wave and L the distance travelled in the plasma, which for our purposes has been approximated to 2 mm, from the data sheet presented by the producer. By defining the theoretical plasma transmitted pulse as:

$$E_{th}(t) = F^{-1}(H(\omega)XS_{ref}(\omega)) \quad (45)$$

With $F^{-1}()$ indicating the inverse Fourier transform, we obtained a numerical THz pulse to be compared with the mea-

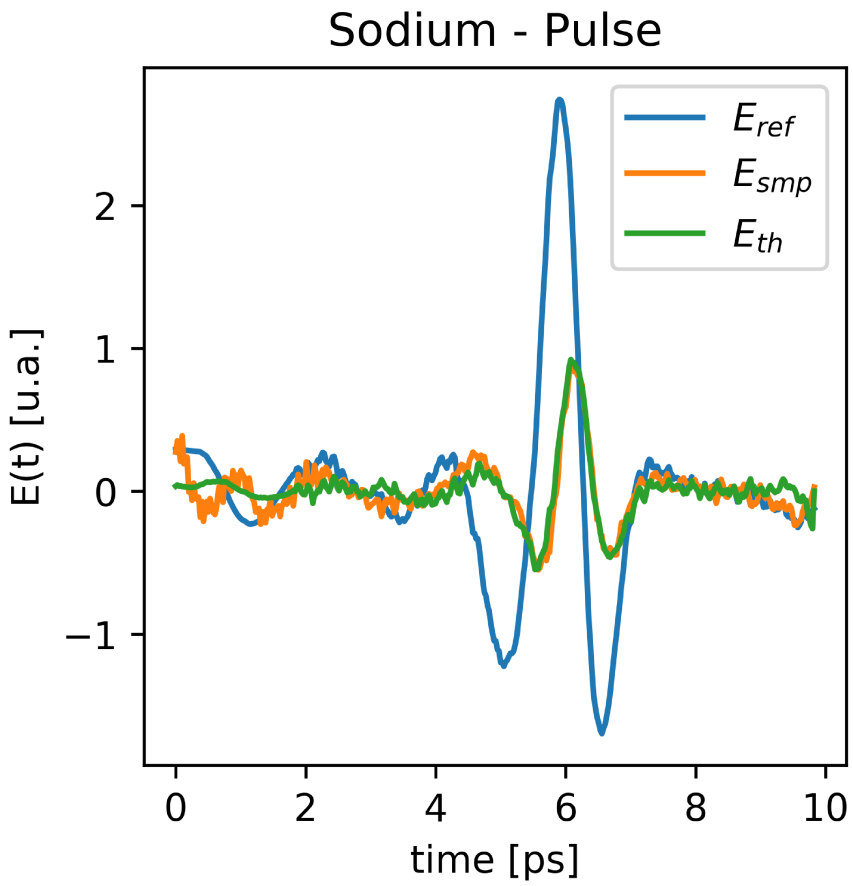

Figure 39: Measurements from the Na lamp 93122E. (E_{ref}) = reference THz pulse measured with hot glass bulb. (E_{smp})= THz pulse during lamp operation. (E_{th})= plasma pulse calculated from analytical model using (E_{ref}) as input.

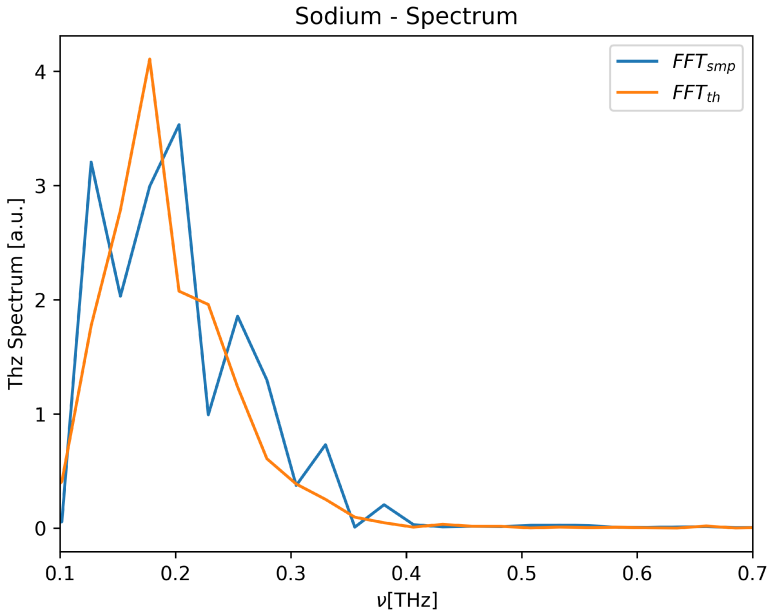

Figure 40: Measurements from the Na lamp 93122E. It is represented the spectrum of the sample and the one derived by the model (FFT_{smp})= THz spectrum during lamp operation. (FFT_{th})= plasma spectrum calculated from analytical model using (FFT_{ref}) as input , not showed for difference intensity scale proportion, having the (FFT_{smp}) spectrum much lower intensity due to glass absorption.

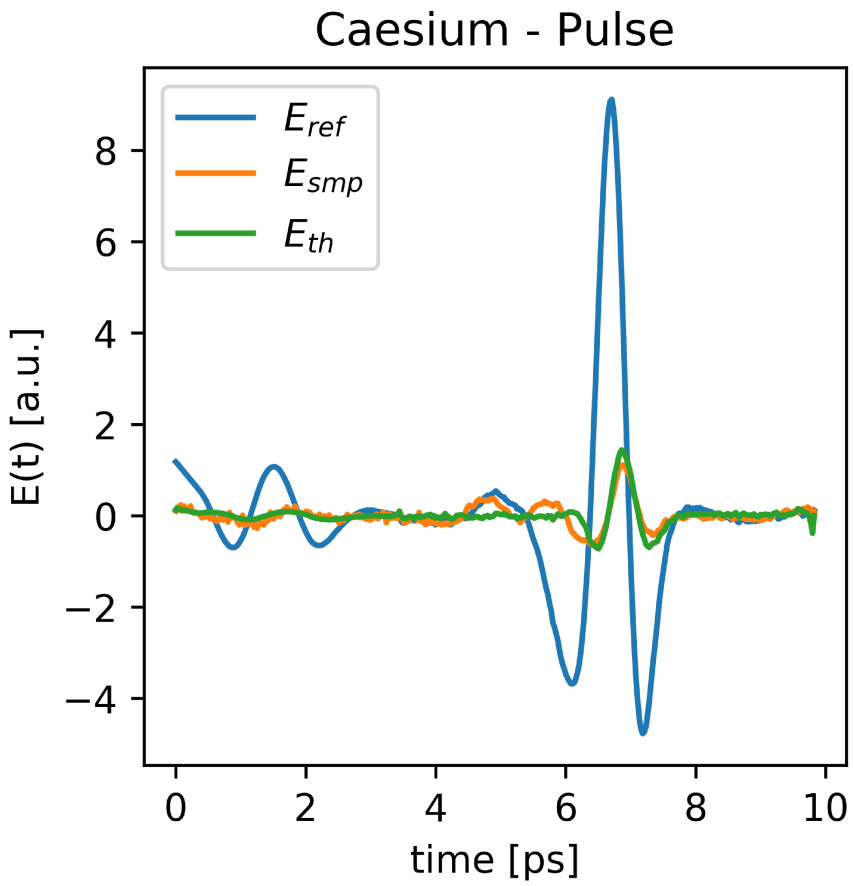

Figure 41: Measurements from the Cs lamp 93105E. (E_{ref}) = reference THz pulse measured with hot glass bulb. (E_{sample})= THz pulse during lamp operation. (E_{th})= plasma pulse calculated from analytical model using (E_{ref}) as input.

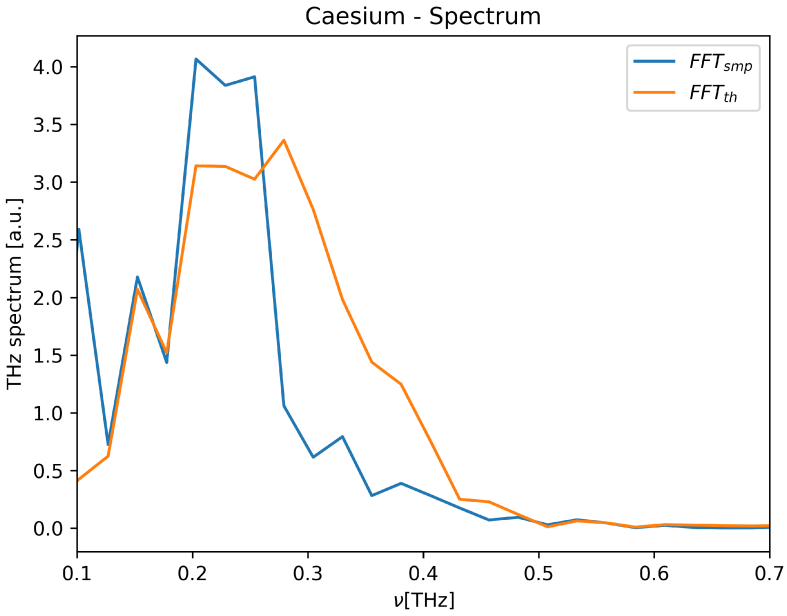

Figure 42: Measurements from the Cs lamp 93105. It is represented the spectrum of the sample and the one derived by the model (FFT_{smp})= THz spectrum during lamp operation. (FFT_{th})= plasma pulse calculated from analytical model using (FFT_{ref}) as input, not showed for difference intensity scale proportion, having the (FFT_{sample}) spectrum much lower intensity due to glass absorption.

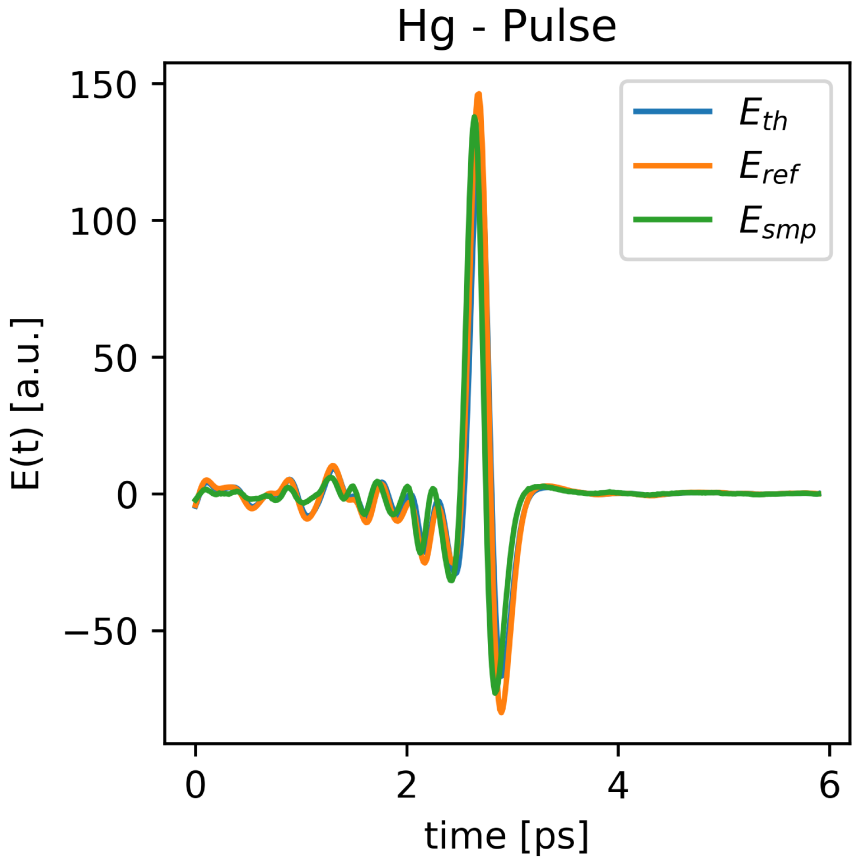

Figure 43: Measurements from the HG lamp HPK125. (E_{ref}) = reference THz pulse measured with hot glass bulb. (E_{smp})= THz pulse during lamp operation. (E_{th})= plasma pulse calculated from analytical model using (E_{ref}) as input.

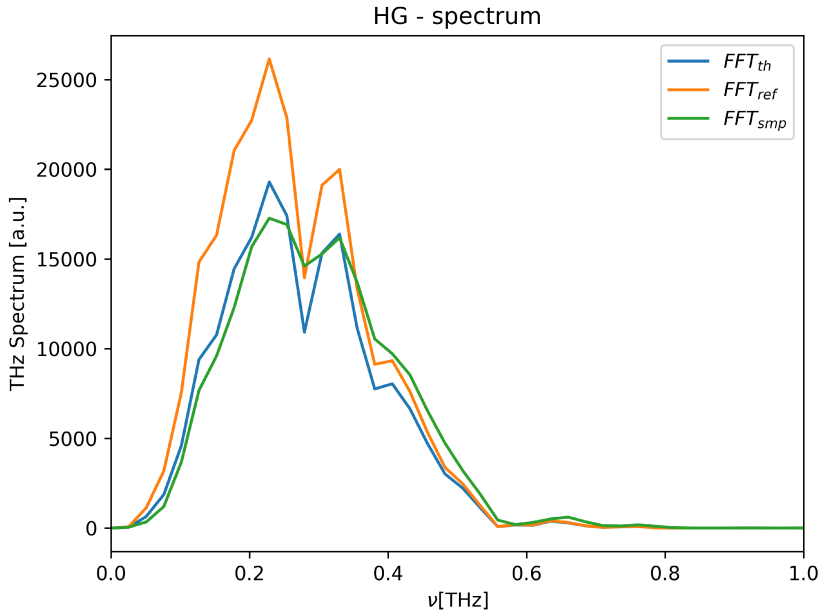

Figure 44: Measurements from the HG lamp HPK125. It is represented the spectrum of the sample and the one derived by the model (FFT_{sample})= THz spectrum during lamp operation. (FFT_{th})= plasma spectrum calculated from analytical model using (FFT_{ref}) as input (Orange). The HPK515 lamp, with only the absorption of one bulb of quartz could give an higher transmitted signal and so with a comparable spectrum with the reference.

sured pulse, and to choose by iteration the best values of n_e and ν_e to minimise the rms value of $E_{th} - E_{smp}$. For each Gas the simulated pulses and spectrum are shown in Figs. 39 40 41 42 43 44 and the fit parameters shown in 4.

Experimental Results

Using this simple analysis method we estimated the parameters of Hg (HPK), Na and Cs plasmas in the spectroscopic lamps, as summarised in Table 4. The values obtained are compatible with the technical specifications of the lamps [56]. One of the main sources of uncertainty was located in the thickness and shape, of the plasma slab. In this demonstration we assumed an approximate guide value based on geometrical considerations. The measured pulse for Hg (9136E), showed in fig. 36, not having a enough resolution was not further analysed.

Lamp Type	$n_e[10^{20}m^{-3}]$	ν_e [THz]
Hg-HPK125	0.4	1.5
Na-93122E	1.9	0.9
Cs-93105E	4.6	1.7

Table 4: Measured characteristics of Philips spectroscopic lamps n_e is the plasma density ν_e the electron-electron collisional frequency.

Conclusions

The experiment successfully performed a preliminary experimental demonstration of the THz-TDS diagnostic potential with a characterisation of spectroscopic lamp plasmas, by using a basic electromagnetic transmission model. By resolving the technical issues that emerged during this work, precision

and accuracy of the measurements will be greatly improved. A suggestion for improvement could take the form of an external cooler for the lamps to extend the measurement time. For specific plasma diagnostics application, such as in tokamaks, the technique may be refined by adopting the well-established data analysis methods and plasma models for the specific diagnostic application [59],[6].

4.8 GROUP VELOCITY DELAY COMPENSATION IN OPTICAL FIBERS OPERATION

4.8.1 *General Description*

The technique of transmitting a laser beam to the THz emitter and receiver wafers by means of fibres, successfully implemented by several authors [41] [60] is particularly interesting for a plasma diagnostics environment where accessibility is a major issue. The prototype scheme is displayed in Figure 45.

The fibre-optics operation is constrained by the optically dispersive properties of the fibres: the different wavelength components travel at different group velocities, in accordance with their respective refractive index within the fibre. This generates an increasing time delay between the different frequencies, known as linear chromatic dispersion. The shorter wavelengths are slower in glass than the longer ones in positive dispersion. Femtosecond pulses have a high bandwidth which enhances the effect further. The input pulse, initially compact, broadens after travelling through the fibre, according to the delay accumulated by each component. THz-TDS measurements become impossible without a suitable compensation set-up of this group velocity delay (GVD). The compensation set-up is achieved by sending the main laser beam through a double

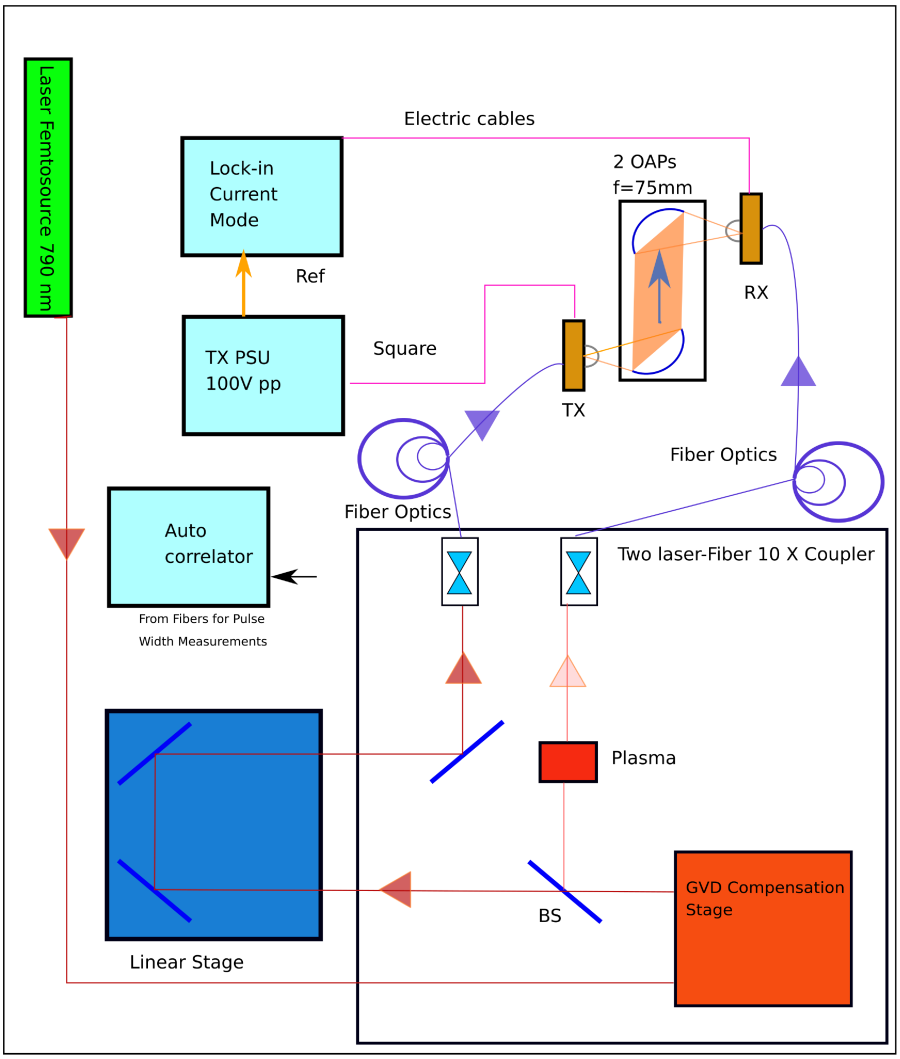

Figure 45: General schematic of a Fiber-Optics THz-TDS Spectrometer for Plasma Diagnostics applications. The Group Velocity Delay compensation section is in the box in the bottom-left (see text for discussion). A femtosecond IR laser pulse is pre-compressed by a pair of holographic gratings before being separated in two beams by a beamsplitter. One beam is delayed by a mechanical delay stage and then pass trough a 5 meter fiber optics and is focalized on a GaS emitter controlled by a high voltage PSU. The other beam pass trough a long optical fiber (5m in our tests) and is focussed on a photoconductive detector, the signal of which is amplified by a lockin synchronised with the PSU square-wave modulation (17 KHz).

grating compression stage, which exhibits negative or anomalous dispersion, to counteract the positive GVD. The beam is separated in its frequencies components by the diffraction grating; a combination of gratings give the possibility to arrange the frequencies distribution (anomalous dispersion) forming a compressed pulse in the time domain. The compressor output beam is divided in two sub-beams (not necessarily of equal power) by means of a beam splitter (BS). One branch is for the Receiver (RX) and the other for the Emitter (TX). The two beams are successively coupled from free space into two long (2m+) optical fibers, applying a 10X microscope stage for each fiber.

We now come to the main drawback of the fibre coupled system, in the context of plasma diagnostic applications. In order to minimise losses, complexity and costs, it would be preferable to use a single GVD compressor for the two beams. This means that since the free-air THz path from TX to RX is part of the TX branch which can be of the order of several meters in tokamak application, a comparably long compensation line is required in the RX branch. Considerable length scales such as this one are a notorious source of opto mechanical complications, normally not present in table-top devices. Another point to consider is that the scanning stages positioning in the TX path must necessarily be after the GVD compressor, and before the laser-fibre coupler. This does not fulfil the requirement of entering the optical fibre as soon as possible after compression, encouraging the unavoidable degradation of the laser beam occurring during compression [61]. Our decision was to start with the single GVD compressor, and evaluate the results for the final diagnostic design.

4.8.2 *Laboratory Tests*

Preliminary tests of the GVD compression scheme were performed at the Clarendon Laboratory in Oxford by using a mode-locked Femtosource 790 nm laser, with nominal 26 fs pulse width, corresponding to 100 nm bandwidth, 75 MHz repetition rate and average output power 480 mW.

The pulse compression scheme relies on two Spectrogon holographic gratings with 1200 grooves/mm, see Figure 46for details. For a given length of optical fibre, a certain laser pulse expansion is produced as shown in Fig 47 . A reliable estimate of the GVD induced by normal fused silica fibers of length L [41] at 800 nm is described by eq. 46 . Without compensation, a 30 fs input optical pulse with a bandwidth of 100 nm broadens to at least 60 ps after travelling through 5 m of fibre. Such a distortion will render the pulse useless for successful THz-TDS applications, and should be counteracted by adequate pre-compression, achieved by tuning the distance between gratings.

$$\Delta\tau = 120 \cdot L \cdot bw \tag{46}$$

With the compressed time pulse length $\Delta\tau$ expressed in fs, the fiber length L in meters and the pulse bandwidht bw in nm.

Promising results have been obtained with 5m single mode optical fiber 780-HP, which has the following specifications:

Operating Wavelength 780-970 nm, Cutoff Wavelength 730±30 nm, Core Diameter 2a= 4.0 µm, Mode-field Diameter $2w_0$= 4.6 µm with $2w_0$ the gaussian beam width, Numerical Aperture NA= 0.14, Refractive Index Value - Core 1.463 651 nm.

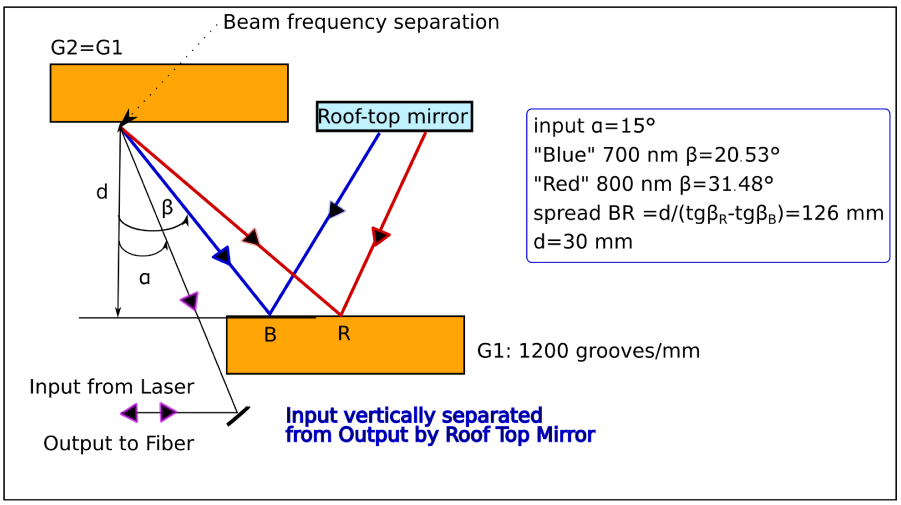

Figure 46: Top view of pulse compression stage schematic, as tested at Clarendon Laboratory. Two holographic gratings Spectrogon 715.700.550 with 1200 grooves/mm and Littrow angle at 780 nm = 27.90 deg provide the required negative dispersion, which compensates for the fiber positive dispersion. The device input and output paths are coincident, since the beam components travels back to themselves after diffraction on the G2 grating and recombine on the first grating (G1) regaining the input beam path. A roof top mirror is then necessary to vertically separate the input and output beams planes so the output can be collected by a Triplet collimator and focussed on a Femtochrome FR-103MC autocorrelator for pulse width measurement. In the final THz-TDS fiber spectrometer configuration the output fiber will be directly connected to the THz Emitter and Receiver units. "Red" and "Blue" wavelengths are symbolic names to refer to the laser pulse spectral limits.

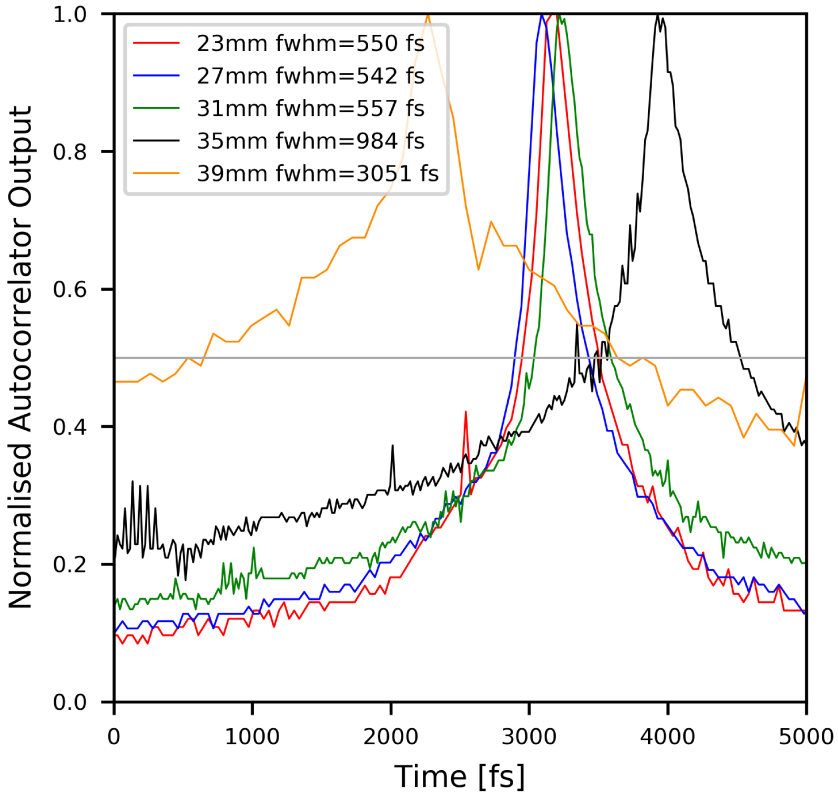

Figure 47: Normalised FWHM pulse width (in fs) measured for different gratings separation at the output of the compression stage (the grey line marc 50 % signal level). As shown in the legend, the optimum compression is achieved for d=27mm, very close to the gratings Litrows angle (where the majority of diffracted power is in the first order of diffraction). The larger grating efficency in this region can be appreciated by the increased SNR for d=27mm.

From eq. (46) the expected pulse widening with this fiber is between $120fs \cdot 5 = 60$ ps, a quantity which is undetectable with the autocorrelator. For this reason, the required optimum compression separation between the gratings, hereby indicated as d (see Figure 47), was estimated using the criteria in [60], obtaining $d = 60$ mm for the initial setup. With systematic scanning of d, optimum compression was obtained for distance $d = 27mm$, for 542 fs FWHM pulse width, equivalent to a compression factor in excess of 100 (see Figure 47). The difference between estimated theoretical and experimental values of d is within the precision range of the estimate, and is accounted for by both the different characteristics of the optical fibers, and extra positive dispersion occurring in components of the system, for example in the triplet collimator and in the gratings glazing. The compressed pulse length achieved in this test (500 fs) is still marginal for THz generation and detection, but constitutes a good experimental demonstration of the feasibility of the technique, given the ample optimisation margins of the system. It should be noted that THz plasma diagnostics rely on the lower part of the THz spectrum, specifically frequencies below 2 THz. This enables investigations experiments using a wider laser pulse (around 100 fs), implying a narrower spectral band and reduced dispersion, and requiring a smaller degree of compensation.

5

CONCLUSIONS AND FUTURE WORK

The work presented in this thesis encompasses three years of intensive research activity aimed to develop a diagnostic for a harsh plasma environment based on the THz-TDS technology.

The bottom line is to adapt the existing well developed THz-TDS technology to perform FIR and submm waves plasma diagnostics measurements with a novel approach, with would overcome the quasi-optical and radio time-domain techniques which have succesfully dominated the last decades of Fusion research, but now approaching the next generation devices, start showing some limitations, especially in terms of plasma access, SNR, calibration and reliability.

To this end a preliminary study of the operational parameters for the best candidates for a THZ-TDS plasma diagnostic system has been realised, with particular reference to FTU Tokamak in Frascati. Interferometry, Reflectometry and Polarimetry have been discussed in details obtaining a full set of instrumental requirements.

Due to the special nature of plasma diagnostic application, the approach amply used by spectroscopic and material study laboratories, consisting of buying commercial device with the desired specifications, and use it for the table top measuremets on the relevant samples, is not viable. A deep understanding of every single aspect of THZ-TDS applications is required to develop and designed a tailored plasma diagnostic facility, hence the first part of the work was dedicated to the development of a THz-TDS laboratory setup in the Frascati Enea laboratory.

Photoconductive detectors, allowing simultaneous dual-polarization measurememements, where studied in depth and valuable experience has been acquired on the assembly, alignment and use of these devices. The more important alignment parameters have been devised and it has emerged that the alignment procedure is critical. For a full exploitation of the photoconductive technique a receiver and transmitter head using Silicon think lenses to pre-focus the THz beam and reduce the alignment criticity will be essential, this will be the subject of one of the most important future developments of ths work.

In order to test sub-sections, single components and materials witout the criticity of the photoconductive systems, a standard THz-TDS Electro Optical setup has been designed and installed in Frascati in collaboration with Oxford Clarendon Laboratory. This will constitute a reliable test bench for every future development of systems and components.

Since the fiber optics operation, main subject of this work, will be essential in Plasma Diagnostics, we developed and tested a tailored pulse compression stage, based on a negative-dispersion gratings pair. The device has been successfully tested at Clarendon and the parameters operational set has been defined. An improved version of the pulse compression stage is in advanced designed stage, and will be installed at ENEA Frascati in completion of the work of this project, as essential milestone towards the Plasma Diagnostic realization.

A complementary line of work was carried away at CIO laboratory (Leon, Mexico) by using the commercial equipment available there, with single polarization photoconductive antenna emitter and detector. The application of the technique to plasma diagnostic relevant measurements was studied for many cases (Poalrimetry, Refraction index, Reflectometry) obtaining many

useful insights from the applications for material and heritage science routinely done at CIO.

Demonstrative plasma measurements have been performed at Clarendon laboratory, using a setup developed and assembled in Frascati to estimate the plasma density inside commercial spectroscopic lamps. Beyond the numerical estimate of the parameters, the tests provided a full-horizon view of the parameters, accuracy, precision and limitation of the technique.

In conclusion the building blocks of a novel THz-TDS multifunctional plasma diagnostic system for Nuclear Fusion research, have been devised, designed and individually tested. A powerful network of laboratories, each one providing a specific set of skills and techniques, has been created. The resulting synergy will be the propulsive force to the final step in the realization of the diagnostic for next step Fusion devices.

BIBLIOGRAPHY

[1] J. Friedberg. *Plasma Physics and Fusion Energy*. Cambridge University Press, 2007.

[2] J Lawson. In: *Proc. Phys. Soc. B 70 6* (1957).

[3] J. Sheffield. "Physics of magnetic fusion reactors." In: *Rev. Mod. Phys* 66.3 (1994).

[4] L. Pieroni. *Internal Report CNEN*. Tech. rep. 77.25/cc. Centro di Frascati, 1977.

[5] M. Bornatici et al. In: *Nucl. Fusion* 23.1153 (1983).

[6] I. H. Hutchinson. *Principles of Plasma Diagnostics*. Cambridge University Press, 2002.

[7] M. Tonouchi. "Cutting-edge terahertz technology." In: *Nature photonics* 1.2 (2007), pp. 97–105.

[8] H.W. Hübers M. Kimmitt E. Bründermann. *Terahertz Techniques*. springer, 2012.

[9] P. Calvani. *Appunti del laboratorio di Fisica della Materia 2001*.

[10] R. Boyd. *Radiometry and the detection of optical radiation*. John Wiley and Sons, 1983.

[11] E. Plyler et al. "Radiant Energy from Sources in the Far Infrared." In: *J. Opt. Soc. Am.* 52.8 (1962), pp. 859–861.

[12] P. Kotthaus. "High Power Output from a Submillimeter cw Gas Laser." In: *Appl. Opt.* 7.12 (1968).

[13] Hubers et al. "Terahertz quantum cascade laser as local oscillator in a heterodyne receiver." In: *Opt. Express* 13.15 (2005).

[14] Auston et al. "Picosecond photoconducting Hertzian dipoles." In: *Applied Physics Letters* 45 (1984), pp. 284–286.

[15] M. Perenzoni. *Physics and Applications of Terahertz Radiation*. Springer Series in Optical Sciences, 2014.

[16] N. Sarukura et al. “High average-power THz radiation from femtosecond laser-irradiated InAs in a magnetic field and its elliptical polarization characteristics.” In: *Journal of Appl. Phys.* 84.11 (1998).

[17] JT Darrow. “Subpicosecond electromagnetic pulses from large photoconducting antenna.” In: *Optics Letters* 15.6 (1990), pp. 323–325.

[18] P. Y. Han et Al. “Coherent broadband midinfrared terahertz beam sensors.” In: *Appl. Phys. Lett.* 73.21 (1998).

[19] A. Nahata et Al. “A wideband coherent terahertz spectroscopy system using optical rectification and electro-optic sampling.” In: *Appl. Phys. Lett.* 69.16 (1996).

[20] Charles A. Schmuttenmaer. “Exploring Dynamics in the Far-Infrared with Terahertz Spectroscopy.” In: *Chem. Rev.* 104.4 (2004).

[21] M. Zerbini et al. “Far Infrared and THz Detectors: Principl es of Operation and Figures of Merit.” In: IEEE Proceedings of 43th IRMMW Conference, Nagoya (Japan), PID5309715. (2018).

[22] S S Dhillon et All. “The 2017 terahertz science and technology roadmap.” In: *J. Phys. D: Appl. Phys* 50.4 (2017).

[23] Shafranov. *Reviews of Plasma Physics*. Vol. 3. Consultants Bureau, 1967.

[24] M. Heald and C. Wharton. *Plasma diagnostics with microwaves*. John Wiley and Sons Inc., 1965.

[25] H. Jeffreys. In: *Proc. London Math. Soc.* 2 (1923).

[26] Hartfuss. “RF techniques in plasma diagnostics.” In: *Plasma Phys. Control. Fusion* 40.8A (1998).

[27] C Laviron. “Reflectometry Techniques for density prifle measurements on fusion plasmas.” In: *Plasma Phys. Control Fusion* 38.7 (1996).

[28] S.H. Heijnen. “Pulsed Radar Reflectometry.” PhD thesis. University of Utrecht, 1995.

[29] A. Tuccillo et al. “Progress on THz Applications for Plasma Diagnostics.” In: IEEE Proceedings of 40th IRMMW Conference, Hong Kong, paper WS-58. 2015.

[30] M.Zerbini et al. “From FIR and millimeter waves to THz plasma diagnostics applications.” In: IEEE Proceedings of 41th IRMMW Conference, Copenhagen (Denmark) paper H5P.26.03. 2016, pp 1–2.

[31] C.W. Domier. “Ultrashort-pulse reflectometry.” In: *Rev. Sci. Instrum* 66.1 (1995).

[32] M. Zerbini et al. “From FIR and Millimeter waves to THz Plasma Diagnostics applications.” In: *International Conference on Infrared Millimeter and Terahertz Waves IRMMW-THz*. Ed. by IEEE Computer Society. Vol. 2016-November. 2016.

[33] J. T. Good. “Design and Applications of a Decade-Spanning Terahertz Frequency Comb Spectrometer: Doppler-limited Rotational Spectroscopy of Methanol and Methanol-OD.” PhD thesis. California Institute of Technology, 2016.

[34] James Lloyd-Hughes. “Terahertz time-domain spectroscopy of carrier trapping in semiconductors.” PhD thesis. Oxford, 2006.

[35] M. B. Johnston et al. “Simulation of terahertz generation at semiconductor surfaces.” In: *Phys. Rev. B* 65 (2002), p. 165301.

[36] J. Xu X. Zhang. *Introduction to THz Wave Photonics*. Springer, 2010.

[37] N. D. Mermin N. W. Ashcroft. *Solid State Physics*. Cengage Learning, 2011.

[38] *Mira 900 Laser Instruction Manual*. 2004.

[39] J. C. Diels. *Ultrashort Laser Pulse Phenomena*. Academic Press, 2006.

[40] E. Castro-Camus. “Polarisation resolved terahertz time domain spectroscopy.” PhD thesis. Condensed Matter Physics Oxford, 2006.

[41] S.A. Crooker. "Fiber-coupled antennas for ultrafast coherent terahertz spectroscopy in low temperatures and high magnetic fields." In: *RSI* 73 (2002), p. 3258.

[42] B. H. Kolner et al. "Time-resolved pulsed-plasma characterization using broadband terahertz pulses correlated with fluorescence imaging." In: *Appl. Phys. Lett.* 87.15 (2005).

[43] *APE auto-correlator manual*. 2000.

[44] A. Rice et Al. "Terahertz optical rectification from (110) zinc-blende crystals." In: *Appl. Phys. Lett.* 64.11 (1994).

[45] mitsui chemicals. URL: https://www.mitsuichemicals.com/tpx.htm.

[46] Alexander Podzorov and Guilhem Gallot. "Low-loss polymers for terahertz applications." In: *Applied Optics* 47 (2008).

[47] G.Galatola Teka. *Spettroscopia TeraHertz per Diagnostiche del Plasma*. Master Degree Thesis, Uniroma1. 2015.

[48] W. Withayachumnankul et al. "Material parameter extraction for terahertz time-domain spectroscopy using fixed-point iteration." In: *Photonic Materials, Devices, and Applications* Proceedings Volume 5840 (2005).

[49] I. Pupeza et Al. "Highly accurate optical material parameter determination with THz time-domain spectroscopy." In: *Optical Society of America* 15.7 (2007), p. 4335.

[50] Scipy Manual.

[51] S. Busch et al. "Optical Properties of 3D Printable Plastics in the THz Regime and their Application for 3D Printed THz Optics." In: *J Infrared Milli Terahz Waves* 35.12 (2014), pp. 993–997.

[52] M. Scheller et al. "Terahertz form birefringence." In: *Optical Society of America* 18.10 (2010), pp. 10137–10142.

[53] S. Jamison et al. "Plasma characterization with terahertz time-domain measurements." In: *J. Appl. Phys.* 93 (2003).

[54] D. Jang K. Kang and H. Suk. "Plasma density measurements using THz pulses from laser-plasmas." In: *Journal of Instrumentation* 12 (2017).

[55] G. Galatola-Teka et al. ""THz-TDS Transmission Measurements of Spectroscopic Lamps Plasma"," in: IEEE Proceedings of 43th IRMMW Conference, Nagoya (Japan), PID5452059. (2018).

[56] W. Elenbaas et al. *Light sources for line spectra*. Tech. rep. Philips Technical Review, 1950.

[57] T. Seifert. "Efficient metallic spintronic emitters of ultrabroadband terahertz radiation." In: *Nature Photonics* 10 (2016), pp. 483–488.

[58] G. Gallot and D. Grischkowsky. "Electro-optic detection of terahertz radiation." In: *Journal of optical society of America* 16.8 (1999).

[59] M. Zerbini et al. F. Causa. "FTU diagnostic system based on THz Time-Domain Spectroscopy." In: *3rd International Conference 'Frontiers in Diagnostic Technologies , ICFDT3 2013*. Ed. by Physics Procedia. Vol. 62. 2015, pp. 66–70.

[60] F. Ellrich et al. "Compact fiber-coupled terahertz spectroscopy system pumped at 800 nm wavelength." In: *Rev. Sci. Instrum.* 82 (2011), p. 053102.

[61] *M. Zerbini, private communication, 2017*.

ACKNOWLEDGMENTS

I desire to thank all the wonderful people that helped me during these three long year, firstly to express my gratitude to my supervisor Marco which guided me giving the insight to avoid mistake and always supporting me with great patience. I would like also to thanks Andrea, Emilio and Gian Piero for the help inside and outside the laboratory and the many interesting conversations. Also i want to remember and thanks Giuliano, Valerio, Franco, Paolo,Luca,Onofrio, Cristina and all the FTU reasearch and tecnichians group that helped or expanded my expertise in many fields during these ears. I would like also to thank my PhD. colleagues and my friends.

I'm deeply grateful to Michael Johnstonand Enrique Castro-Camus for the help and the precious time had inside their laboratory.

Last but not the least I would like to thank my family, my mother and my father.